LBL-16261
c.2

Lawrence Berkeley Laboratory

UNIVERSITY OF CALIFORNIA

RECEIVED
LAWRENCE
BERKELEY LABORATORY
APR 17 1984
LIBRARY AND
DOCUMENTS SECTION

Materials & Molecular Research Division

MECHANISMS OF MICROSTRUCTURALLY-INFLUENCED FATIGUE CRACK GROWTH IN DUAL-PHASE STEELS

V.B. Dutta
(M.S. Thesis)

June 1983

TWO-WEEK LOAN COPY

This is a Library Circulating Copy which may be borrowed for two weeks. For a personal retention copy, call Tech. Info. Division, Ext. 6782.

Prepared for the U.S. Department of Energy under Contract DE-AC03-76SF00098

LBL-16261
c.2

DISCLAIMER

This document was prepared as an account of work sponsored by the United States Government. While this document is believed to contain correct information, neither the United States Government nor any agency thereof, nor the Regents of the University of California, nor any of their employees, makes any warranty, express or implied, or assumes any legal responsibility for the accuracy, completeness, or usefulness of any information, apparatus, product, or process disclosed, or represents that its use would not infringe privately owned rights. Reference herein to any specific commercial product, process, or service by its trade name, trademark, manufacturer, or otherwise, does not necessarily constitute or imply its endorsement, recommendation, or favoring by the United States Government or any agency thereof, or the Regents of the University of California. The views and opinions of authors expressed herein do not necessarily state or reflect those of the United States Government or any agency thereof or the Regents of the University of California.

LBL-16261

MECHANISMS OF MICROSTRUCTURALLY-INFLUENCED FATIGUE CRACK GROWTH IN DUAL-PHASE STEELS

Vivek Brata Dutta

Materials and Molecular Research Division, Lawrence Berkeley Laboratory,
and Department of Materials Science and Mineral Engineering,
University of California, Berkeley, CA 94720

June 1983

M.S. Thesis

MECHANISMS OF MICROSTRUCTURALLY-INFLUENCED FATIGUE CRACK GROWTH IN DUAL-PHASE STEELS

Vivek Brata Dutta

Materials and Molecular Research Division, Lawrence Berkeley Laboratory,
and Department of Materials Science and Mineral Engineering,
University of California, Berkeley, CA 94720

ABSTRACT

Mechanistic implications associated with resistance to fatigue crack growth in three different microstructures of dual-phase Fe/2Si/0.1C steel have been examined. The tests have been conducted at both near-threshold ($\leq 10^{-6}$ mm/cycle) and high ($\sim 10^{-6}$-10^{-4} mm/cycle) growth rates as well as at low and high load ratios. The above tests have been accompanied by fatigue crack closure measurements at different stress intensities, ΔK. Both fine globular and coarse dual-phase structures demonstrate exceptionally high resistance to crack growth at near-threshold and mid-growth regions - perhaps the highest ever observed in steels. The crack growth resistance has been observed to be closely related to fracture surface roughness and crack closure levels. The implications of such observations have been discussed in terms of four mutually competitive mechanisms, namely, roughness induced closure, roughness + plasticity induced closure, crack deflection and intrinsic microstructural characteristics.

MECHANISMS OF MICROSTRUCTURALLY-INFLUENCED FATIGUE CRACK GROWTH IN DUAL PHASE STEELS

TABLE OF CONTENTS

	Page
ABSTRACT	1
NOMENCLATURE	iv
1. INTRODUCTION	1
1.1. Significance of Fatigue Threshold	1
1.2. Review of Microstructural Influence on ΔK_o	2
1.3. Characteristics of Dual-Phase Steels	5
1.4. Objective of the Present work	6
2. EXPERIMENTAL PROCEDURE	7
2.1. Material Preparation	7
2.2. Heat Treatment	7
2.3. Machining	8
2.4. Mechanical Testing	8
2.4.1. Tensile Testing	8
2.4.2. Fatigue Crack Propagation	9
2.4.3. Crack Closure Measurements	11
2.5. Optical Metallography	12
2.6. Scanning Electron Microscopy (SEM)	13
3. RESULTS	14
3.1. Mechanical Properties	14
3.1.1. Uniaxial Tensile Tests	14
3.1.2. Fatigue Crack Propagation	14
3.1.3. Crack Closure Measurements	15

TABLE OF CONTENTS (Cont.)

Page

3.2. Metallography 15

3.2.1. Crack Profile (Optical) 15

3.2.2. Quantitative Metallography 17

3.3. Fractography 18

4. DISCUSSION 19

4.1. Influence of Microstructure at Low Load Ratio (R = 0.05) . 19

4.1.1. Near-Threshold Region 19

4.1.2. Mid-Growth Region 21

4.2. Influence of Microstructure at High Load Ratio (R = 0.75) . 23

4.3. Evidence Supporting Influence of "Crack Deflection" 24

4.3.1. Premature Crack Retardation - A Deflection Effect . 26

4.4. Relative Dominance of Different Mechanisms of Fatigue Crack Growth 27

4.5. Microstructural Influence on Crack Geometry 27

5. CONCLUSION 30

ACKNOWLEDGEMENTS 32

REFERENCES 33

TABLES 37

FIGURES 39

NOMENCLATURE

a	length of the main crack
a_0	initial crack length
a_p	projected crack length from the tip
a_T	total length of the crack surface from the notch tip
D	length of the deflected segment
S	length of the linear segment
θ	angle of deflection from the plane of maximum tensile stress
W	specimen width
B	specimen thickness
α	crack length to specimen width ratio
P_{max}	maximum applied load during fatigue cycle
P_{min}	minimum applied load during fatigue cycle
P_{cl}	load corresponding to crack closure in a fatigue cycle
ΔP	applied load range
K_{max}	maximum stress intensity during fatigue cycle
K_{min}	minimum stress intensity during fatigue cycle
K_{cl}	stress intensity to cause fatigue crack closure
K_{eff}	effective stress intensity factor
ΔK	stress intensity range ($K_{max} - K_{min}$)
ΔK_{eff}	effective stress intensity range ($K_{max} - K_{cl}$)
ΔK_o	threshold stress intensity range for no crack growth
ΔK_I	nominal Mode I stress intensity factor range
$\overline{\Delta K_I}$	average stress intensity factor range in a segment
γ	non-dimensional surface roughness factor
x	ratio of Mode II to Mode I displacement

R	load ratio (K_{min}/K_{max})
R_{cr}	critical load ratio above which roughness-induced crack closure cannot occur
da/dN	fatigue crack growth rate per cycle
dc/dN	nominal crack growth rate
$\overline{dc/dN}$	average growth rate of a deflected crack

1. INTRODUCTION

1.1. Significance of Fatigue Threshold

It is well established that fatigue crack propagation rates (da/dN) of a microscopically long crack can be characterized in terms of the alternating stress intensity factor, ΔK.[1] In steels, this results in a sigmoidal variation in growth rate with respect to ΔK, demonstrating three regimes with characteristic primary crack growth mechanisms, Fig. 1.[2] The very low crack growth rates, below 10^{-6} mm/cycle, as represented in Regime A, have lately been of particular interest to investigators. Here the local crack growth rates approach a single lattice spacing per cycle. The corresponding stress intensity range is referred as the so-called threshold value ΔK_0, below which cracks remain dormant or propagate at experimentally-undetectable rates.

When the concept of threshold and ultra-low propagation rate data are utilized with the defect tolerance approach in design or for fracture control procedures in situations involving high frequency/low amplitude loadings, the distinct lack of reliable engineering data has been a considerable limitation. Nevertheless, the use of such data has been found to be vital in applications such as large scale nuclear and coal conversion pressure vessels, turbine shafts, turbine blades, alternator rotors, aircraft structures, chattering of tandem cold mill rolls and acoustic fatigue of welds in gas circulators of nuclear reactors where high frequency low amplitude loading conditions may prevail.[2]

1.2. Review of Microstructural Influence on ΔK_0

Recent studies have shown that near-threshold crack growth rates are sensitive to several mechanical and microstructural variables, such as mean stress or load ratio, residual stresses, frequency, environment, monotonic and cyclic yield strength, crack size, grain size, inclusions, etc. Among the microstructural variables, the grain size has received much attention from several investigators.[3-18] At low growth rates and low load ratios, several workers[3,6,7,13.14,17] have observed improved resistance to near-threshold crack propagation with coarser grain sizes. Generally speaking, both ferrite and prior austenite grain size appear to demonstrate the same trend.[3,14] However, in high strength steels a decrease in ΔK_0 with increasing prior austenite grains is observed.[4] In most of the studies, the crack profile near threshold is found to be associated with a rough and zig-zag growth. The degree of roughness seems to increase with grain size. Various explanations have been provided supporting such observations of roughness, grain size and threshold ΔK_0. Masounave and Bailon[3] have considered near-threshold growth confined to specific crystallographic planes. As a result, in coarse structures greater deviation of the crack path from the plane of maximum tensile stress takes place. According to Lucas and Gerberich[6] the grain size effect is attributed to sub-grain cell structure. Lindigkeit et al.[61] used the slip reversibility argument where the resistance to crack propagation is considered to be due to decrease in the rate of accumulation of dislocation locally ahead of the crack tip. During the unloading part of the cycle the dislocations are expected to move backwards in coarse

grains. Such a phenomenon is restricted in smaller grain sized materials due to secondary slip planes in the same or adjacent grains. For high strength steels this effect is explained through generation of atomic hydrogen at the crack tip.[10,11] On the other hand, for high strength steels where a decrease in crack growth rate near threshold with smaller grain size has been observed by Carlson and Ritchie,[4] the effect of grain refinement to improve resistance to crack propagation has been considered as a possibility.

As a consequence of these micromechanisms which are possibly occurring near the threshold region, an increased near-threshold crack growth resistance can be explained due to possible closure effects,[22,53,55] where some closure of the crack surface may take place at positive loads during the unloading cycle. As the load ratio is increased, however, the crack remains open during the majority of the cycle and the role of crack closure is expected to diminish significantly.[2,5,7,12]

The grain size to yield strength relation in steel is well understood. Also, evidence has been provided[15,16] showing that increasing the yield strength of steel decreases its threshold values. As a result, if a coarse grained material is used for better resistance to fatigue crack growth applications, the strength has to be sacrificed or vice versa. In most cases a compromise is the only solution. However, recent investigations carried out on dual-phase steels (ferrite, α + martensite, α')[8,19-21] have revealed several interesting phenomena related to the significance of microstructure in controlling fatigue crack growth in the near-threshold region. It introduces a

very promising way of improving the fatigue threshold of low carbon steels without compromising other mechanical properties. Suzuki and McEvily[19] observed in AISI 1018 steel, a dual phase microstructure with continuous martensite network results in an increase in strength and threshold level as compared to a continuous ferrite network. The continuous α' network was suggested to exert a strong constraint upon the degree of plastic deformation at a crack tip resulting in smaller plastic zone size and hence higher ΔK_0. Such effects have further been investigated for a number of steel compositions and microstructures.[20] These authors have attributed high ΔK_0 values for duplex α' network structure due to the tortuous path taken by crack front near-threshold and corresponding closure effects. Such effects become less pronounced with an increase in martensite volume fraction. The results of Wasynczuk[21] demonstrate that threshold stress intensities for fatigue crack growth in AISI 1018 dual phase steels are unaffected by changes in the distribution and volume fraction of martensite and σ_y. However, comparing with a different steel (Fe/2Si/0.1C), having a similar microstructure, higher threshold is observed. This steel demonstrates a rougher crack path. The high threshold is attributed to possible roughness induced crack closure.[22] A consistently common feature observed in all the above mentioned works is that in Regime A the crack grows through both ferrite and martensite phases.

The results of different dual phase microstructures discussed so far are difficult to compare. Besides different distributions and volume fractions and α and α' phases, the important variables such as grain size and strength were not always controlled, thus possibly

influencing the results. Further, all the tests were performed at low load ratios (characterized by $R = K_{min}/K_{max}$), where closure mechanisms [5,22,54] are suggested to predominate near the threshold. Therefore, the conclusions are likely to suppress the understanding of any other mechanism, if associated with microstructure. Hence the existing information does not permit one to perceive all the mechanistic aspects of microstructure during crack extension under cyclic loading. It necessitates further insight, which could possibly lead to setting guidelines for designing superior fatigue resistant microstructure of dual-phase steels.

1.3. Characteristics of Dual-Phase Steels

The characteristic features of dual-phase ($\alpha + \alpha'$) microstructure are that they contain ferrite (α) as the ductile matrix with strong and tough second phase of low carbon martensite (α').[23,24] Dislocated martensite is preferred for obtaining optimum properties.[25] Such a structure gives highly desirable tensile properties, such as continuous yielding from a low yield strength, high initial strain hardening rates and excellent combination of ultimate tensile strength with ductility.[26-29] Several workers[26-38] have correlated structure (volume fraction, shape, size and distribution of second phase) - property (monotonic tension, hardness, Charpy impact, fractography, S-N curves for fatigue) of dual phase steels and the results are well established.

In the present work, to study the effect of phrases on fatigue crack growth, Fe/2Si/0.1C steel has been selected. The tests are performed on three types of dual phase microstructures viz. intermediate quenched, step quenched and intercritically annealed.[30]

1.4. Objective of the Present Work

In light of the above discussions, it is clear that with the limited extent of information available in the literature, it is not possible to make any viable mechanistic interpretation of microstructural influence of dual phase steels on fatigue crack propagation rate.

The purpose of the present work is therefore to:

(i) establish reliable data base for programming a controlled experiment (where the variables such as grain size and yield strength are fixed) to understand the mechanism of microstructurally-influenced fatigue crack growth;

(ii) obtain guidelines to design a superior fatigue resistance microstructure.

2. EXPERIMENTAL PROCEDURE

2.1. Material Preparation

The material chosen for this investigation was Fe/2Si/0.1C steel, the nominal composition of which is given in Table I. The material was supplied by Sandia National Laboratory, Albuquerque, New Mexico, and designated as 12-1-38. The vacuum induction melted steel was fully killed with rare earth and cast in 23 kg (50 lb) ingot. The as cast ingot was vacuum arc remelted and homogenized at 1100°C for 16 hours in an argon-atmosphere. The ingot was then hot-forged in the 850°-1050°C range to 76.2 mm (3 inch) square bars and controlled rolled (from 950°C to 790°C) to 13.3 mm (0.525 inch) thick plate before being received at Berkeley. Oversized compact tension and tensile blanks were removed from the plate in L-T orientation. The blank dimensions were approximately 12.7 mm × 70 mm × 76 mm (½ in × 2 3/4 in × 3 in) and 12.7 mm × 12.7 mm × 70 mm (½ in × ½ in × 2 3/4 in), respectively.

2.2. Heat Treatment

All the blanks were wrapped in stainless steel packets and homogenized at 1200°C for 20 hrs and air cooled to ambient temperature, in order to (a) ensure same microstructure and grain size to start with and (b) protect the blanks from surface oxidation and decarburization. Dual-phase, ferrite + martensite, microstructures were obtained through three different heat treatment cycles, viz. intermediate quenching (IQ), step quenching (SQ) and intercritical annealing (IA), as shown in Figure 2(a). Based on the available information,[30] the exact time-temperature parameters of these cycles were established through trial and error

such that the variation of yield strength of the materials with three different microstructures is minimum. Also, in order to obtain the same prior austenite grain size, the austenitizing time and temperature were kept constant for all three cycles. The heat treatments of dual-phase structures were performed in an electrical resistance vertical tube furnace under argon atmosphere. The blanks (two numbers of compact tension and one tensile - per set), pertaining to a heat treatment cycle, were simultaneously treated.

2.3. Machining

Both the tensile and compact tension (CT) specimens were finally machined following heat treatment by removing a surface layer of 3.2 mm from all faces and edges. The purpose of this machining was to minimize any influence of residual stress due to heat treatment.[40] Care was taken with the depth of cut and cooling in order to refrain from generation of any localized stress during machining.

2.4. Mechanical Testing

2.4.1. Tensile Testing

Cylindrical sub-size tensile specimens of 12.7 mm gauge length and 3 mm gauge diameter, in accordance with ASTM specification E8-69,[41] were used (Fig. 3(a)). The loading direction of the specimen was kept perpendicular to the rolling direction of the material. Tests were conducted at room temperature using a 'TT Floor Model Instron screw machine (44.4 kN capacity), with a crosshead speed of 0.05 mm/sec and a full scale load of 910 kg. The engineering yield strength was

determined as 0.2% offset value. Four specimens were tested for each heat treatment.

2.4.2. Fatigue Crack Propagation

Compact tension specimens in L-T orientation, as per ASTM Standard 399-78a,[39] has been used (Fig. 3(b)). Fatigue crack propagation experiments were performed on a 98 kN electro-servo-hydraulic MTS testing machine operating under load control and 9.8 kN range. Tests were conducted at room temperature (22°C) and laboratory air. The frequency used was 50 Hz and wave shape was sinusoidal. Crack growth was monitored using dc electrical-potential technique[43-46] capable of detecting increments in crack length of the order of 0.01 mm. The experimental setup is demonstrated in Figure 4. Near-threshold growth rates were approached using a load-shedding (decreasing stress intensity) technique in which a procedure of successive load (or ΔK) reduction, initially in decrements of 10% and near ΔK_o, in decrements of 5%, followed by crack growth was performed. Details of this experimental procedure have been described elsewhere.[2,21,47,48] The tests were conducted at load ratios ($R = K_{min}/K_{max}$) of 0.05 and 0.75 where K_{min} and K_{max} are the minimum and the maximum stress intensities during each cycle. The stress intensity range ΔK was determined using the following expression:[42]

$$\Delta K = \frac{\Delta P(2 + \alpha)}{B\sqrt{W}\,(1 - \alpha)^{3/2}} (0.886 + 4.64\alpha - 13.32\alpha^2 + 14.72\alpha^3 - 5.6\alpha^4)$$

where ΔP - applied load range

B - specimen thickness

W - specimen width

and $\alpha = a/W$, i.e., the crack length to width ratio; this expression is valid for $a/W \geq 0.2$.[52]

During load changing, the actual ΔK was calculated at the corresponding crack length a, determined from electrical potential calibrations.[44-46] In order to minimize premature crack arrest and crack growth retardation effects due to residual compressive stresses generated in front of the crack tip, the crack length increments - over which measurements of growth rate are taken - were kept at least four times larger than the monotonic plastic zone size generated at the previous load level. The threshold stress intensity, ΔK_o, was defined at the highest alternating stress intensity at which no crack growth could be detected within 10^7 cycles, or in terms of a maximum crack growth rate of 10^{-8} mm/cycle.[2] For each fatigue test a pair of fatigue crack growth rate, da/dN vs. alternate stress intensity, ΔK curves were obtained, referring to low and high load ratios. It is important to note that the projected crack length ($a_o + a_p$) is considered for ΔK calculations. The total length of crack surface ($a_o + a_T$) provides only an indication of the 'degree of roughness,'* when compared to projected length for different crack profiles. The differences in these crack lengths, which is a consequence of fracture surface roughness, is schematically shown in Fig. 5.

In the present set of experiments, the near-threshold growth data were obtained at two different load ratios from the same fatigue test. The specimens were first subjected to low R (= 0.05) and ΔK corresponding to mid-growth regime. Once the threshold was obtained at low R, both K_{max} and K_{min} were readjusted for high R (= 0.75). Then, by

---

*Degree of roughness, as presented in Table III, is defined as the percentage change in projected crack length due to roughness and is expressed as $((a_T - a_p/a_p) \times 100)$, where a_T = total length of crack surface and a_p = projected crack length.

subsequent load shedding - in decrements of 5% - the near-threshold regime data were obtained at high R. Once the threshold was reached, keeping the same K_{max}, the K_{min} was reduced corresponding to R = 0.05. Then by incremental load-shedding mid-growth range data were obtained. The tests were terminated at ΔK corresponding to the crack growth rate of 10^{-4} mm/cycle. Using this procedure, two specimens were tested for each heat treatment in order to cross check the results.

2.4.3. Crack Closure Measurements

A set of six strain gages were fixed in pairs at three locations on the compact tension (CT) specimen such that at each point one gage records strain parallel and the other perpendicular to the loading axis. The gages were of CEA-06-062WT-120 specification, 1200 ± 0.5/Ω with a gage factor of 2.10. The two flat faces and the back face of the test specimens were chosen for gage fixing. The gage leads were connected to the strain meter at constant temperature (22°C) throughout the test. Details about the setup is elaborated in the schematic diagram (Fig. 6(a)) and actual arrangement (Fig. 7). The entire setup is completed before commencing fatigue crack growth experiments. Zero setting with respect to dummy gage was performed. With the fatigue test in progress, strains were measured corresponding to a wide range of ΔK from mid-growth regime to near-threshold.

When strain measurements for a specific ΔK were to be performed, the MTS machine was parked idle at zero span. The load limits P_{max} and P_{min} for that ΔK was determined. Corresponding to one cycle, the machine load was first increased and then decreased manually. At small increments of loads, between $P_{min} \rightarrow P_{max} \rightarrow P_{min}$, the strain at each gage

was recorded. Relative strain vs. load plots were obtained for each gage, as shown in Figure 6(b). The load corresponding to the change in slope of the curve gives the closure load, P_{cl}. A mean of P_{cl} obtained from the narrowest scatter of six such values was considered for calculating K_{cl}.

2.5. Optical Metallography

Three specimens were removed from every CT specimen once the fatigue test was completed. Two of these specimens were prepared for surface and cross section metallography so that the homogeneity of microstructure and volume fraction of ferrite and martensite phases could be investigated. The third specimen contained the entire crack path, from the notch to the crack tip at the end of the test. This specimen was prepared with the objective to estimate the true crack profile length as compared to point-to-point direct crack length (refer to Section 2.4.2) and also to observe the characteristics of fatigue crack path at different ΔK values. Due precautions were taken while sectioning and polishing these specimens in order to protect the crack profiles from getting damaged. Both etched and unetched micrographs were obtained. 5% Nital was used as etchant. In order to estimate the prior austenite grain size, an intermediate quenched specimen was polished and attacked with ferric chloride etchant (6.25% $FeCl_3$ + 18.75% HCl + H_2O).[49]

Quantitative metallography techniques[50,51] were employed to determine the volume fraction of the two phases, ferrite particle size and prior austenite grain size. The total length of meandered crack

surface was measured from X80 times magnified image using a marker chain. A Ziess Amtex optical microscope was used.

2.6. Scanning Electron Microscopy (SEM)

After optically investigating the crack profile, the cracked specimens were broken open in liquid nitrogen for studying the fracture surface aspects and variation in fracture mode during crack growth at different ΔK values. The observations were made using AMR-1000 and ISI-DS-130 scanning electron microscopes (SEM), operating at 20 and 25 kV, respectively.

3. RESULTS

3.1. Mechanical Properties

3.1.1. Uniaxial Tensile Tests

The engineering stress-strain curves for three different microstructures are shown in Figure 8. The yield strength of the three microstructures vary in a close range from 590 MPa to 635 MPa. Consistent with previous investigations[30] the shape of the step quenched curve demonstrates the highest strain hardening rate and highest tensile strength while the intermediate quenched structure shows the opposite. The intercritically annealed structure has properties in between these two. The tensile test data are given in Table II.

3.1.2. Fatigue Crack Propagation

The fatigue crack propagation curves (da/dN vs. ΔK) for IQ, SQ and IA microstructures are summarized in Figure 9. The curves are plotted for both high ($R = 0.75$) and low ($R = 0.05$) load ratios and the threshold values at high and low load ratios for the three types of microstructure are given in Table III. Referring to the data at $R = 0.05$, in the mid-range of growth rates, the Paris law relationship[1] applies and the slope of IQ and SQ are found to be almost parallel while the IA has a steeper slope. The respective slopes, as determined from crack growth curves (Fig. 9), are shown in Table III. The SQ and IA curves intersect, demonstrating the same crack growth in mid-growth region, at $\Delta K \sim 26$ MPa$\sqrt{m}$.

3.1.3. Crack Closure Measurements

The K_{cl} values at different ΔK were obtained for each microstructure. The relations obtained between ΔK and K_{cl}/K_{max} are shown in Figure 10. It should be noted that when no closure had been observed for certain ΔK (i.e., the elastic compliance curve of Figure 6b has a constant slope) the corresponding K_{cl} was considered as 'zero.' Hence, Figure 10 shows that crack closure was not observed at R = 0.75. In low load ratios (R = 0.05) the closure phenomenon rapidly increases as ΔK approaches threshold ΔK_o. Near-threshold, maximum closure was observed in step quenched structure ($K_{cl}/K_{max} \simeq 0.83$) and minimum for intermediate quenched structure ($K_{cl}/K_{max} \simeq 0.74$). The closure level of intercritically annealed structure was inbetween ($K_{cl}/K_{max} \simeq 0.78$), but had a steeper decline with increasing ΔK. The IA and SQ closure curves intersect at $\Delta K \simeq 25.5$ MPa$\sqrt{m}$.

3.2. Metallography

3.2.1. Crack Profile (Optical)

The crack profiles (both etched and unetched) of the three microstructures are presented in Figure 11. During the fatigue test, premature retardation in crack propagation rate had been observed under standard load shedding procedure. At these points, crack growth rates decreased abruptly below 10^{-6} mm/cycle at relatively high ΔK. Such relevant points are shown on the crack paths with an asterisk (*). Arrows on the crack paths indicate corresponding ΔK at different load ratios. These premature crack growth retardation and ΔK_o points for intermediate quenched, step quenched and intercritically annealed structure, at higher magnification, are shown in Figures 12a-c, 13a-e

and 14a-e, respectively. Each feature is presented in unetched condition to observe the crack shape and the etched condition to observe the influence of microstructure. The following interesting features could be observed from Figures 11 to 14:

(a) The crack propagates in the ferrite as well as martensite, independent of the applied ΔK or load ratio and as such have no preference for either of the two phases. Such an observation is common in all three microstructures.

(b) Crack deflections, i.e., meandering from the plane of maximum tensile stress, have been observed in all three microstructures at mid-growth and near-threshold regions. However, the degree of deflection (viz. kinked length and angle) varied significantly from one structure to another (ref. Figs. 15 to 17).

The intermediate quenched structure shows few such deflections and comparatively smooth crack path. The step quenched structure shows the roughest and the most tortuous crack path. Here the crack deviates significantly from the plane of maximum tensile stress. Such effect is more pronounced near threshold (at both high and low R). The intercritically annealed structure showed roughness inbetween the above two structures, with an increasing trend as the threshold ΔK_0 was approached. The indication of a 'degree of roughness' (as defined earlier) of individual structure is presented in Table III.

(c) All the premature crack growth retardation points and both the thresholds at low and high load ratios, corresponding to the three different crack profiles, are found to be associated with the deflected regions of crack path. However, the crack profiles (Fig. 11) show many other deflected regions where crack growth retardation was not observed.

(d) The etched microstructures of step quenched (Figs. 13 and 16) and intercritically annealed (Figs. 14 and 17) materials revealed that ferrite/ferrite or ferrite/martensite interfaces are preferred crack deflection sites. Some exceptions (Fig. 16a and b) do show deflection within a ferrite or martensite for step quenched material. Such features were not observed in intermediate quenched material (Figs. 12 and 15).

3.2.2. Quantitative Metallography

Figure 2b demonstrates the etched microstructures obtained from the three heat treatment cycles of dual-phase steel. The light and dark areas refer to ferrite (α) and martensite (α'), respectively. Table IV presents the quantitative metallography results viz. prior austenite grain size, ferrite particle size and volume fraction of martensite of the three heat treatments. It should be observed that since all three heat treatments had the same austenitizing temperature (1150°C) and time (60 min), the prior austenite grain size is considered to be the same. As a result, the presented data refer to the observations made on the intermediate quenched microstructure.

3.3. Fractography

The representative fatigue fractograph of the three microstructures are shown near-threshold ΔK_0 (Fig. 18) and mid-growth region (Fig. 19). Essentially, a cleavage type transgranular mode at near-threshold levels could be distinguished from typical "hill-and-valley" type facets. At near-threshold stress intensities, the SQ shows (Fig. 18c) maximum coarseness of fracture surface topography and appear to be consisting of so-called "shear facets."[20] Such facets are not so prominent in the IQ and IA structure. Although the IA structure (Fig. 18e) does not show a very coarse topography, a continuous deflection in the crack face is observed. The IQ shows a comparatively less rough surface (Fig. 18a). In the mid growth region, the SQ continue to show similar characteristics as near threshold while IA and IQ are fairly smooth as compared to near-threshold. The observations under scanning electron microscopy are in close agreement with optical microscopic analysis.

4. DISCUSSION

From the current studies on fatigue crack propagation in dual-phase steel, it is apparent that any variation in microstructure has a remarkable influence on resistance to fatigue crack growth. By suitably designing a microstructure, the threshold ΔK_o could be increased without altering the yield strength of the material. This effect is predominant both in the near-threshold and mid-growth regions.

In the present investigation, microstructural influences have been observed in IQ, SQ and IA structures in Fe/2Si/0.1C steel having similar yield strength and prior austenite grain size. This approach is considered appropriate in order to understand the exact mechanisms associated with microstructures in influencing fatigue crack growth. Contributions due to any variation in yield strength and grain size -- which play very important roles on fatigue crack propagation[2,3,5,6,17] -- may not enable unequivocal interpretation of results.

4.1. Influence of Microstructure at Low Load Ratio (R = 0.05)

4.1.1. Near-Threshold Region

The current results reveal that IA and SQ microstructures have almost two fold increase in threshold values (ΔK_o = 17.1 $\sim$ 19.5 MPa$\sqrt{m}$) as compared to IQ structure (Fig. 9 and Table III). To the author's knowledge, this is the highest threshold ever observed in a low strength steel. The differences in threshold ΔK_o of the three microstructures are in experimental analogy with crack closure measurements (Fig. 10 and Table III).

During fatigue crack growth, some closure of the crack faces may occur at positive loads of the loading cycle.[47,53,59] It implies that, should physical contact between the mating crack surfaces occur at positive loads of a fatigue cycle as a result of the local fracture process, the driving force for crack extension would be effectively limited at the crack tip. The result of this is a reduction in the stress intensity range, responsible for crack propagation, from a nominal value ΔK (= $K_{max} - K_{min}$) to an effective value ΔK_{eff} (= $K_{max} - K_{cl}$), where K_{cl} is the stress intensity to close the crack and is $\geq K_{min}$. The significance of crack closure in influencing fatigue crack growth has long been known.[2,65] Accordingly, several "microscopic" mechanisms of closure have been identified based on the role of:

(a) plasticity induced in the wake of an advancing crack[53] (plasticity-induced crack closure);

(b) corrosion debris formed on the fracture surface[47,54,62] (oxide-induced crack closure);

(c) fracture surface asperities[55,56] (roughness induced crack closure).

The effect of oxide and roughness is prevalent near-threshold stress intensities due to the single shear (Mode I + Mode II) character of the crack extension mechanisms[54-56,64] and from the small magnitude of the associated crack tip opening displacements.

These mechanisms may operate alone or in combination in order to reduce fatigue crack growth rate. However, the metallographic and fractographic features obtained after threshold tests (Figs. 11 to 14 and 18) exhibit that as the crack growth rate approaches threshold, the

crack becomes increasingly rougher and tortuous. Therefore, it is apparent that the closure levels observed near threshold is pertinent to "roughness induced crack closure."

Comparison of the different levels of crack closures (K_{cl}/K_{max}) at threshold (Fig. 10) and relative crack surface asperities (Figs. 12b, 13d and 14c) of the three microstructures reveals that with increasing crack asperities there is an increase in closure level. This observation supports the two-dimensional geometric model[22] for predicting crack closure near-threshold due to fracture surface roughness. The model expresses crack closure as:

$$K_{cl}/K_{max} = \sqrt{\frac{2\gamma x}{1 + 2\gamma x}}$$

where K_{cl} = stress intensity to close crack,

K_{max} = maximum stress intensity,

γ = average height/width of crack asperity,

and x = Mode II/Mode I displacement.

From the above results and discussions it can be inferred that microstructure could be suitably designed to promote rougher crack paths. Such a geometry aids roughness-induced crack closure to play a vital role in improving the near-threshold ΔK_o.

4.1.2. Mid-Growth Region

A particularly striking difference in the crack growth rate (above 10^{-6} mm/cycle) of the three microstructures (Fig. 9) is supported by the corresponding crack closure results (Fig. 10) and crack path roughness

(Fig. 11) at similar nominal ΔK. This could lead to the inferrence that closure due to crack geometry continues to play a dominant role in controlling the crack growth rate at mid-growth region. Mechanisms like roughness-induced crack closure may be activated at the larger ΔCTOD's associated with crack growth at such high ΔK levels,[59] provided sufficient degree of faceted fracture morphology exists. However, such an effect is most prevalent at near-threshold stress intensities. Also, at mid-growth region, where plane stress conditions often exist, plasticity in the wake of the crack tip is likely to influence fatigue crack closure. Nevertheless, Elber's concept[53] needs to be extended further in order to explain the roughness dependence of closure at higher ΔK. The following explanation has been suggested:

Mechanisms underlying plastic deformation due to residual stretch of material in the wake of an advancing crack are well understood.[53,56] If the crack face is smooth -- without kinks (as in the case of the IQ structure) -- such deformation would then be identical on the two faces of the crack, i.e., a mirror image. However, when a rough crack surface occurs as observed in microstructurally sensitive materials, viz. IA and SQ structures, the deformation is not likely to be the same on the two faces. As a result, in the decreasing part of the cyclic loading a mismatch could be created between the two faces causing crack closure. For the same nominal ΔK these closure values are expected to increase with an increase in fracture surface roughness and a decrease in yield strength of the microstructural phases forming those asperities.

Similar agreement between the experimental data suggests that a rough crack geometry -- which presumably causes crack closure due to

heterogeneous plastic flow in crack asperities -- contribute in reducing crack propagation rate in mid-growth region.

4.2. Influence of Microstructure at High Load Ratio (R = 0.75)

As the load ratio is raised to R = 0.75, the near-threshold fatigue data (excluding the influence of crack deflection, which will be discussed later) for the three microstructures (Fig. 9) exhibit a considerable decrease in ΔK_o values. The fact that the concurrent closure measurements confirm $K_{cl}/K_{max} = 0$ apparently indicates that minimum stress intensity K_{min} has exceeded K_{cl} and the crack remains open during the entire loading cycle. Therefore, critical load ratio for these structures R_{cr} is ≤ 0.75, where the near-threshold growth is not influenced by closure. However, at this stage reasons for the narrow range of variation in ΔK_o values of the three structures, appear to arise from crack deflection (a situation where the effective crack driving force is presumably governed by the "intrinsic characteristic of the individual microstructure").

In such drastically varying microstructures of the same material (where the crack geometry is influenced and non-continuum mechanism of growth prevails) there exists a likelihood that certain "intrinsic microstructural characteristics" exert considerable influence. These could be: (a) micro-residual stresses; (b) effective shear stresses within the slip plane; (c) interface characteristics between ferrite/ ferrite and ferrite/martensite interphases as well as within each phase, and (d) reactivity of each structure to environment. An analysis of the tangible contribution of each of these factors towards effective ΔK and crack growth rate, however, is beyond the scope of the present work.

4.3. Evidence Supporting Influence of "Crack Deflection"

Characterization of fatigue crack advance under nominally Mode I loading conditions is generally based on the premise that the path of the crack is linear and that its plane of growth is normal to the loading axis. However, as observed in the present experiment using IQ, SQ and IA structures, pronounced deflection or branching of the crack can occur due to local microstructural discontinuities. These results along with several existing evidence indicate that deflections in crack profile can cause marked alteration in fracture behavior in certain cyclic loading situations where crack growth along the deflected trajectory occurs over several thousand cycles. Under such circumstances, both the value of the stress intensity factor (computed from a linear crack profile) and the measured crack propagation rates (which ignore deflection in crack path) are substantially in error. The role of fatigue crack growth under purely tensile (Mode I) external (far-field) loading condition has recently been examined by Suresh[57] and models have been suggested to predict fatigue crack growth rates for various degrees of deflection. Variation in fatigue growth behavior arising from the tilted crack can be estimated knowing the angle of deflection (θ), length of deflected segment (D) and length of linear segment (S). The effective driving force is then expressed as

$$\overline{\Delta K_I} = (D\Delta K_{eff} + S\Delta K_I)/(D + S)$$

where ΔK_I is nominal Mode I stress intensity factor range

and ΔK_{eff} is effective stress intensity factor range controlling crack growth rate.

Corresponding measured average crack growth rate:

$$\left(\frac{\overline{dc}}{dN}\right) = \left(\frac{D\cos\theta + S}{D + S}\right)\left(\frac{dc}{dN}\right)$$

The predicted variations in fatigue behavior arising from deflection are compared here with the present experimental results (Fig. 20). The IQ structure leads to a predominantly linear crack profile during fatigue cycling. The fatigue behavior for this heat treatment is modelled as a reference for an undeflected crack ($\theta \approx 0$) in Figure 20. Changing the heat treatment of this steel to obtain SQ structure has been observed to cause pronounced deflections in crack path during the entire range of fatigue crack propagation (Fig. 11). A typical example of the tortuous crack path for this material is illustrated in Figure 16e which shows the crack profile with deflection at $\Delta K \approx \Delta K_o$. Considering the pronounced deflections in crack path in the SQ structure and taking typical values of angles of tilt $\theta \approx 45°-75°$ (occurring over several grains through the specimen cross section) and $\frac{D}{D + S} \approx 0.25-0.5$, it can be inferred from the model that the remainder of the differences in the fatigue behavior of these two materials is accounted for by crack deflection phenomena.

For each microstructure (Fig. 11), the influence of deflection on resistance to crack growth is evident from the corresponding fatigue curves (Fig. 9). The curve shifts to the right as the 'degree of roughness' increases. Thus, non-linearities in crack path seem to cause a substantial influence on the *apparent* fatigue growth characteristics (consistent with the predictions of the deflection models), in

addition to the effects of the ensuing crack closure and intrinsic microstructural factors.

4.3.1. Premature Crack Retardation - A Deflection Effect

It follows from the above discussion that pronounced crack deflection during fatigue can lower the stress intensity range to such an extent that significant retardation in crack growth rate (or even complete crack arrest) can occur at high nominal ΔK. Such transient retardations in crack growth rate have been observed in the current investigation -- at times even in mid-growth regions. These anomalous and unreproducible results are invariably traced back to be associated with crack deflections. The asterisks (*) in Figures 11 to 14 represent such points along with corresponding nominal ΔK values.

This localized crack growth retardation is an important characteristic of microstructurally sensitive materials which promotes a rough and tortuous path. Therefore, considering material selection purely based upon fatigue crack resistance properties, although IA has the highest resistance until an applied $\Delta K \sim 26$ MPa$\sqrt{m}$, the SQ could be more favorable, since it shows the maximum probability of a high ΔK_o in real application. This offers an additional safety factor from the defect tolerance point of view.

In terms of recommended procedures for measuring near-threshold fatigue crack growth and threshold ΔK_o values, such transient retardations could have important consequences -- especially while testing microstructurally sensitive materials. If and when such localized regions arise, it is suggested to increase nominal ΔK adequately (thus involving variable amplitude loading) and reobtaining the data points by subsequent standard load shedding procedure.

4.4. Relative Dominance of Different Mechanisms on Fatigue Crack Growth

So far evidence has been provided to understand the mechanism of microstructurally-influenced fatigue crack growth in dual-phase steel. It is suggested that the crack growth rate is controlled by the following four mechanisms which appear to have various degrees of influence on the three microstructures and at different growth conditions.

(a) Roughness induced closure operative near threshold and at low load ratios. Its relative influence is SQ > IA > IQ.

(b) Crack closure at mid-growth range, possibly due to plastically damaging crack faces, causing mismatch. Effective at low load ratios. The influence is IA > SQ > IQ (at $\Delta K \leq 26$ MPa$\sqrt{m}$) and SQ > IA > IQ (at $\Delta K \geq 26$ MPa$\sqrt{m}$).

(c) Crack deflection effects operative through Regimes I and II and at different load ratios. Here, IA > SQ > IQ.

(d) Intrinsic microstructural characteristics in both the regimes and is independent of the load ratio. Here, IA > SQ > IQ.

4.5. Microstructural Influence on Crack Geometry

The current investigation suggests that the effect of closure and deflection on fatigue crack growth rate is fundamentally linked with a rough crack surface. An attempt has been made to understand the possible mechanisms underlying such characteristic microstructural sensitivity towards cyclic loading conditions, based upon the metallographic and fractographic evidence (Figs. 11 to 19) of the three different microstructures of dual-phase steel.

In the *near-threshold region* the roughness asperities have been well documented by a number of investigators.[3,7,17,19-21,55,60,61,63] Crack growth in this region is suggested to be confined to specific crystallographic planes[3] and hence depends upon grain-to-grain orientation. As a result, in coarse structures greater crack asperities (i.e., a rougher crack path) would be more favorable. Therefore, in each microstructure it is necessary to consider the different regions with the same orientation. Table IV shows SQ having very large size ferrite particles (103 μm), thus explaining the possible reason for its characteristic roughness asperities. However, a similar argument fails to explain the increase in crack asperities near-threshold in IA structure where ferrite particle size is rather small (27 μm).

In the *mid-growth region*, although plastic zone size is very large and the possibility of occurrence of a single slip system is rather remote, the SQ structure continues to demonstrate a very rough crack path (Figs. 11, 16 and 18). There exists a possibility that large size martensite particles (Fig. 2b) cause constraints at the crack tip. The effect of hard second phase particle on plastic zone size and shape has been well documented.[58] It is likely that due to the presence of coarse martensite in continuous ferrite (the microstructural feature of SQ structure) a similar effect might prevail under certain distributions of martensite particles. This could lead the crack to deflect from the plane of maximum tensile stress. Deflection at high growth rates could also be due to twinned martensite or interlath retained austenite -- which would introduce weak directional properties in the local crack vicinity. Presence of such phases have been documented in the SQ structure.[30]

The foregoing discussion emphasizes the importance of microstructure of dual-phase steels, which significantly influences crack closure and deflection mechanisms during fatigue crack propagation. Based upon this study it has been possible to design microstructures viz. IA and SQ which demonstrate exceptionally high resistance to fatigue crack growth both at near-threshold and mid-growth regions. Such improvements are the highest ever observed in steels.

5. CONCLUSIONS

Based on a study of the effect of dual-phase microstructures on fatigue crack growth in Fe/2Si/0.1C steel, the following conclusions may be drawn:

(1) For a constant yield strength and prior austenite grain size, the fatigue crack propagation rate is greatly influenced by different microstructural shape, size and distribution of ferrite and martensite. Such effects are relevant to near-threshold as well as in mid-growth regions.

(2) Microstructural effects on fatigue crack growth appear to be more pronounced at low load ratios. Crack closure seems to support such observation.

(3) Fracture surface roughness plays a dominant role in influencing fatigue crack resistance of a microstructure.

(4) Crack deflection is expected to contribute in reducing crack growth rate in Regime A and Regime B.

(5) In low load ratios and near-threshold the closure phenomena appear to be due to roughness induced crack closure, where contributions due to Mode II displacement is significant in causing mismatch between fracture surfaces.

(6) In low load ratios and mid-growth region, the closure observed is attributed presumably to the mismatch caused by heterogeneous plastic deformation behind the crack tip.

(7) Differences in fatigue curves at high load ratio tend to suggest that certain intrinsic microstructural characteristics viz. micro-residual stresses, effective shear stresses within the slip

planes, coherency of interface between ferrite and martensite particles and reactivity of each structure to environment -- whose tangible contribution is not investigated -- apparently play an important role in governing fatigue crack growth rate.

(8) A material, with favorably distributed large size second phase particles, could promote premature crack arrest even at mid-growth region. From the defect tolerance approach such microstructure may be considered more appropriate for fatigue crack resistance applications.

(9) The microstructures designed through intercritical annealing (IA) and step quenching (SQ) heat-treatments of low carbon dual phase steel exhibit the highest resistance to fatigue crack growth ever observed in steels, without compromising on yield strength values.

ACKNOWLEDGEMENTS

The author extends his appreciation to Professor Robert O. Ritchie for the encouragement he gave in initiating this investigation and the valued advice rendered subsequently. Special thanks are also extended to Professor Gareth Thomas and Professor Shiro Kobayashi for their suggestions while reviewing the manuscript.

The author is grateful to Dr. S. Suresh for his guidance and support throughout the course of this investigation. Valuable discussions with Dr. Nack-Joon Kim, Alvin Nakagawa, Jye-Len Tzou and other colleagues are also acknowledged. The support of the technical staff of the Materials and Molecular Research Division (MMRD) was invaluable. Profuse thanks are extended to Madeleine Penton who transformed the manuscript into a wonder work of art.

The author is greatly indebted to his wife, Milu, who, besides providing continuous encouragement, editorial assistance and bearing patience, had also provided financial support to sustain the family during this period. Thanks are extended to his children - Debolina and Abhik - who unknowingly contributed in making the dark days of research seem brighter.

This work was supported by the Director, Office of Energy Research, Office of Basic Energy Sciences, Material Science Division of the U.S. Department of Energy under Contract No. DE-AC03-76SF00098.

REFERENCES

1. P. C. Paris and F. Erdogan, J. Basic Eng. (Trans. ASME, D), 1963, 85, p. 528.

2. R. O. Ritchie, Intern. Met. Rev., 20, 1979, p. 205.

3. J. Masounave and J.-P. Bailon, Scripta Met., 10, 1976, p. 165.

4. M. F. Carlson and R. O. Ritchie, Scripta Met., 11, 1977, p. 1113.

5. C. J. Beevers, Fatigue Thresholds, Proc. 1st Int. Conf., Stockholm, Sweden, EMAS Publ. Ltd., Warley, 1981, Vol. 1, p. 257.

6. J. P. Lucas and W. W. Gerberich, Mat. Sci. & Eng., 51, 1981, p. 203.

7. G. T. Gray, III, A. W. Thompson, J. C. Williams and D. H. Stone, Fatigue Thresholds, Proc. 1st Int. Conf., Stockholm, Sweden, EMAS Publ., Warley, 1981, Vol. 1, p. 345.

8. T. Kunio, M. Shimizu, K. Yamada and H. Nakabayashi, ibid., p. 409.

9. D. Taylor, ibid., p. 455.

10. J. D. Frandsen and H. L. Marcus, Scripta Met., 9, 1975, p. 1089.

11. R. O. Ritchie, Fracture 1977, ed. D. M. R. Taplin, Vol. 2, p. 1325, 1977, Waterloo, Ontario, University of Waterloo Press.

12. A. J. Cadman, C. E. Nicholson and R. Brook, Fatigue Thresholds, Proc. 1st Int. Conf., Stockholm, Sweden, EMAS Publ., Warley, 1981, Vol. 1, p. 293.

13. P. E. Irving and C. J. Beevers, Mat. & Eng., 14, 1974, p. 229.

14. J. P. Bailon, J. Masounave and J. Lanteigne, Scripta Met., 12, 1978, p. 607.

15. O. Vosikovsky, Eng. Fract. Mech., 11, 1979, p. 595.

16. R. O. Ritchie, Jnl. of Eng. Materials & Tech., 99, Series H, 1977, p. 195.

17. E. K. Priddle, Scripta Met., 12, 1978, p. 49.

18. S. Taira, K. Tanaka and M. Hoshina, ASTM STP 675, 1979, p. 135.

19. H. Suzuki and A. J. McEvily, Metall. Trans. A, 10A, 1979, p. 475.

20. K. Minakawa, Y. Matsuo and A. J. McEvily, Metall. Trans. A, 13A, 1982, p. 439.

21. J. A. Wasynczuk, M.S. Thesis, University of California, Berkeley, LBL-15110, June 1982.

22. S. Suresh and R. O. Ritchie, Metall. Trans. A, 13A, 1982, p. 1627.

23. J. Y. Koo and G. Thomas, Formidable HSLA and Dual-Phase Steel, AIME, A. T. Davenport ed., New York, 1979, p. 40.

24. R. H. Hoel and G. Thomas, Scripta Met., 15, 1981, p. 867.

25. G. Thomas, Steel, McGraw Hill Yearbook Science and Technology - 1979.

26. J. Koo, Ph.D. Thesis, University of California, Berkeley, LBL-6657, August 1977.

27. N. J. Kim, Ph.D. Thesis, University of California, Berkeley, LBL-12661, September 1981.

28. G. R. Speich, Fundaments of Dual-Phase Steel, R. A. Knot and B. L. Bramfitt, eds., AIME Publ., 1981, p. 3.

29. S. S. Hensen and R. R. Pradhan, ibid., p. 113.

30. N. J. Kim and G. Thomas, Metall. Trans. A, 12A, 1981, p. 483.

31. P. E. Repas, SAE Technical Paper Series 79008, Detroit, 1979.

32. Y. Tomota, N. Tachibana and K. Kuroki, Trans. ISIJ, 18, 1978, p. 251.

33. A. M. Sherman and R. G. Davies, Int. J. Fatigue, January 1981, p. 36.

34. Y. Tomota and I. Tamura, Tetsu-to Hagane (in Japanese), 68, 1982, p. 1147.

35. Y. Tomota and I. Tamura, Trans. ISIJ, 22, 1982, p. 665.

36. C. A. N. Lanzillotto and F. B. Pickering, Mat. Sci., 16, Aug. 1982, p. 371.

37. P. Uggowitzer and H. P. Stuewe, Mat. Sci. & Eng., 55, 1982, p. 181.

38. A. F. Szewczyk and J. Gurland, Metall Trans. A, 13A, 1982, p. 1821.

39. ASTM designation E 399-78a.

40. R. J. Bucci, ASTM STP 743, 1981, p. 28.

41. ASTM Standard E 8-69.

42. ASTM Standard E 647-81.

43. R. O. Ritchie, Tech. Report., Dept. of Metallurgy and Mat. Sci., University of Cambridge, Jan. 1972.

44. R. O. Ritchie and K. J. Bathe, Int. Journ. of Fracture, 15, 1979, p. 47.

45. R. O. Ritchie, G. G. Garrett and J. F. Knott, Int. J. Fract. Mech., 7, 1971, p. 462.

46. G. H. Aronson and R. O. Ritchie, J. Test. Eval., 7, 1979, 208.

47. S. Suresh, Sc.D. Thesis, MIT, May 1981.

48. R. O. Ritchie, Met. Sci., 11, 1977, p. 368.

49. T. Maki and I. Tamura, Tetsu-to-Hagane (in Japanese), 67, 1981, p. 852.

50. E. E. Underwood, ASM Handbook, 8, 1961, p. 37.

51. ASTM Standard E 112-80.

52. J. E. Strawley, Int. Journ. of Fracture, 12, 1976, p. 475.

53. W. Elber, ASTM STP 486, 1971, p. 280.

54. S. Suresh, G. F. Zamiski and R. O. Ritchie, Metall. Trans. A, 12A, 1981, p. 1435.

55. K. Minakawa and A. J. McEvily, Scripta Met., 15, 1981, p. 633.

56. N. Walker and C. J. Beevers, Fat. Eng. Mat. Struct., 1, 1979, p. 135.

57. S. Suresh, University of California, Berkeley, Report No. UCB/RP/83/A1011, submitted to Metall. Trans. A, 1983.

58. M. Sarikaya, A. K. Jhingan and G. Thomas, Met. Trans. A, 14A (in press).

59. R. O. Ritchie, University of California, Berkeley, Report No. UCB/RP/82/M1002, to be published in the "Encyclopedia of Materials Science and Engineering," ed., M. B. Bever, Pergamon Press, Oxford and New York, 1983.

60. P. J. E. Forsyth, Acta Met., 11, 1963, p. 703.

61. J. Lindigkeit, G. Terlinde, A. Gysler and G. Lutjering, Acta Met., 27, 1979, p. 1717.

62. D. Benoit, R. Namdar-Irani and R. Tixier, Mat. Sci. & Eng., 45, 1980, p. 1.

63. G. T. Gray, III, J. C. Williams and A. W. Thompson, Metall. Trans. A, 14A, 1983, p. 421.

64. D. L. Davidson, Fat. Eng. Mat. Struct., 3, 1981, p. 229.

65. R. A. Schmidt and P. C. Paris, ASTM STP 536, 1973, p. 79.

66. J. C. Newman, Jr., ASTM STP 748, 1981, p. 53.

Table I: Composition of Fe/2Si/0.1C Steel

Elements	C	Si	Mn	S	P	Cr	Ni	Mo	V
wt. %	0.09	2.01	<0.005	<0.005	0.005	<0.005	0.06	0.03	<0.01

Table II: Tensile Test Results

Material Structure	Yield Strength MPa	Tensile Strength MPa	% Reduction in Area
Intermediate Quenching	590	805	70.8
Step Quenching	635	900	33.2
Intercritical Annealing	615	827	52.9

Table III: Fatigue Test Results

Material Structure	Near-Threshold ΔK_o (MPa$\sqrt{m}$)		Paris Law Exponent* m	Degree of Roughness **	K_{cl}/K_{max} at ΔK_o (R=0.05)
	Low R (= 0.05)	High R (= 0.75)			
IQ	10.7	4.9	4.8	3.26	0.74
SQ	17.1	5.1	5.3	15.41	0.83
IA	19.5	5.7	9.3	8.49	0.78

*Derived from crack growth data at R = 0.05 above 10^{-6} mm/cycle by regression fit to Paris relationship:

$$\frac{da}{dN} \propto (\Delta K)^m \quad .$$

**Degree of Roughness = $[(a_T - a_p)/a_p] \times 100$.

Table IV: Quantitative Metallography Results

Material Structure	Martensite Vol. Fract. (%)	Ferrite Particle Size µm	Prior Austenite Grain Size µm
IQ	58	9	237
SQ	32	103	237
IA	44	27	237

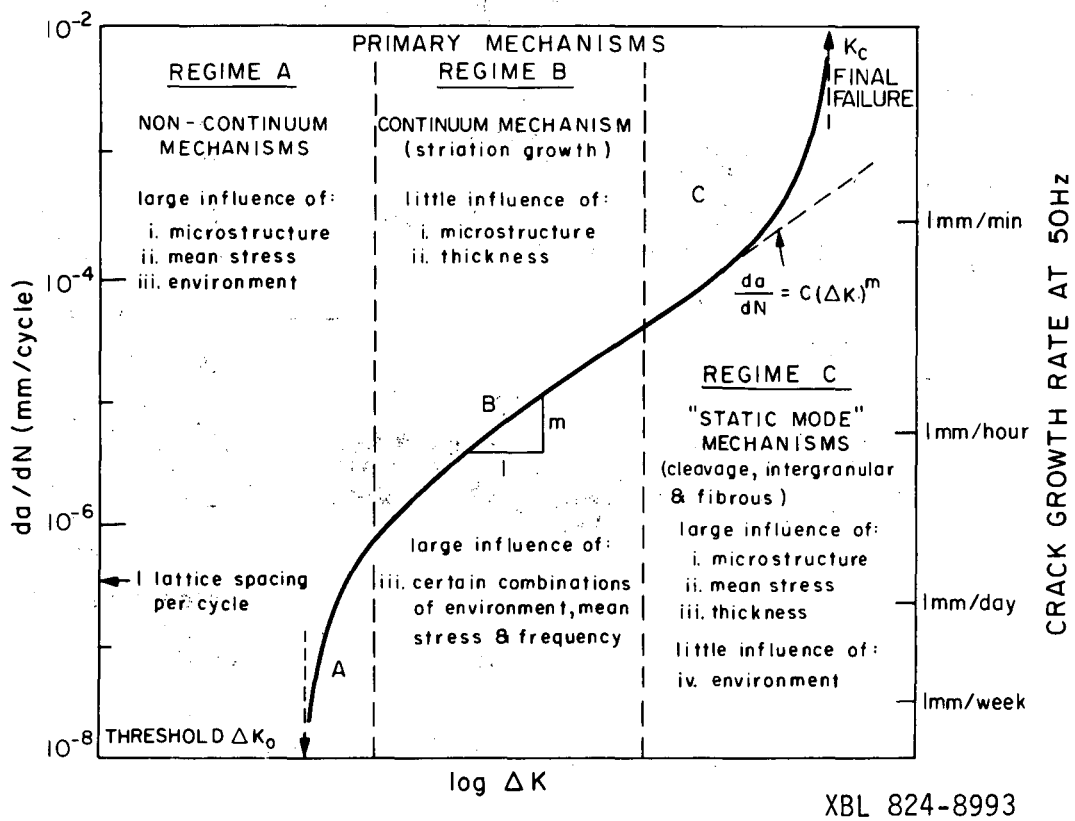

Fig. 1. Schematic variation of fatigue crack growth rate with stress intensity range of steels (ref. 47).

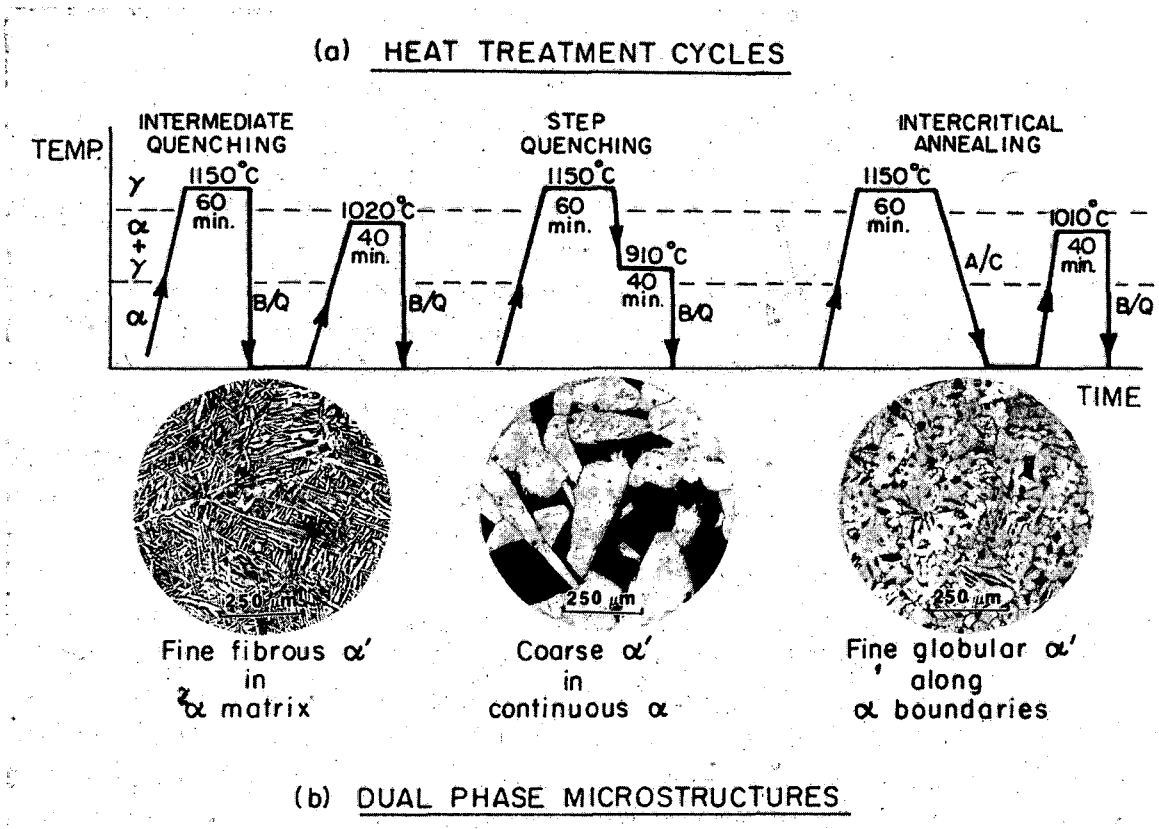

XBB 833-2300

Figure 2. Dual-Phase Fe/2Si/0.1C steel. (a) Heat treatment cycles; (b) optical micrographs.

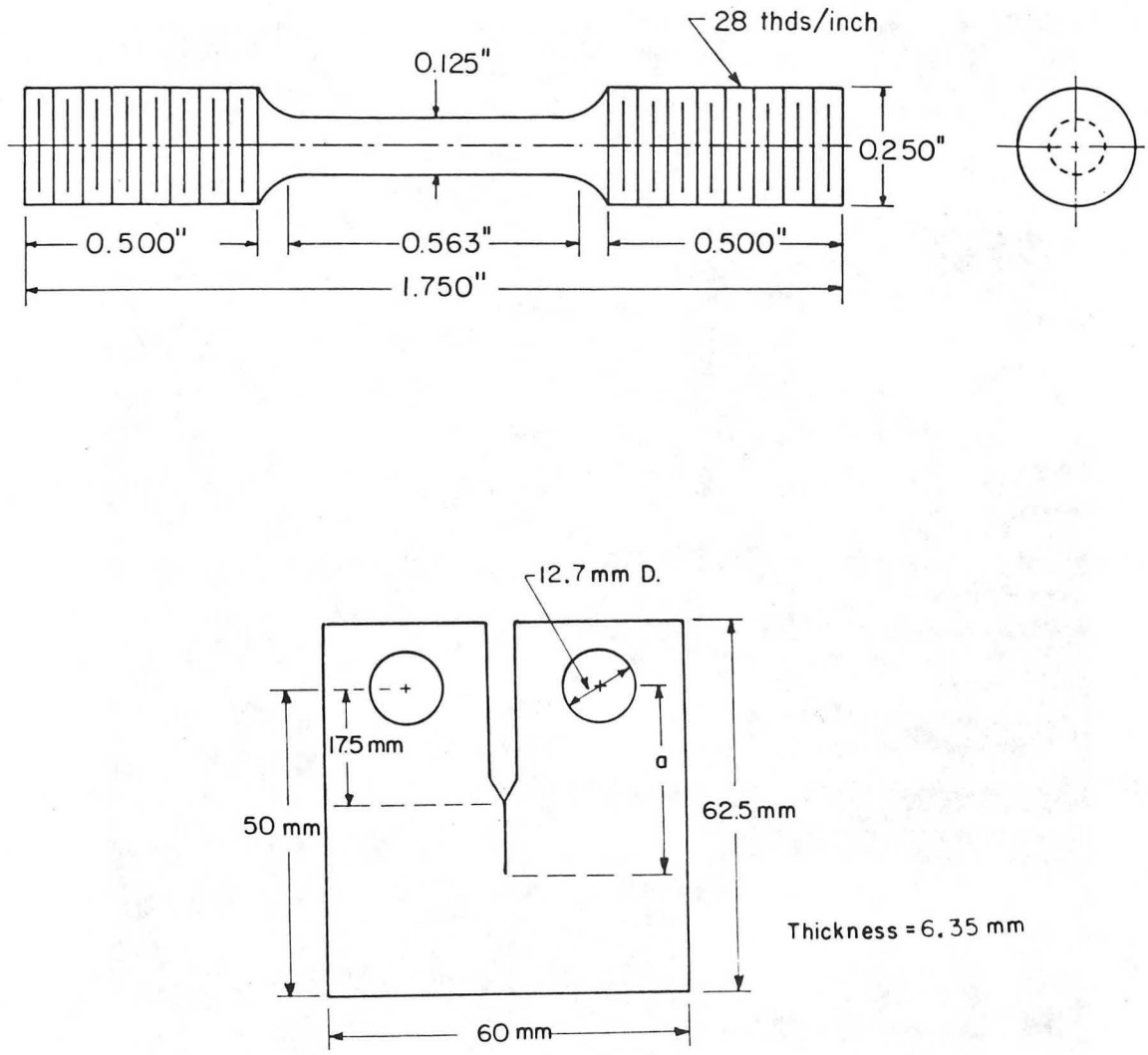

Figure 3. Dimensions of (a) subsize cylindrical tensile test specimen and (b) compact tension specimen for fatigue test.

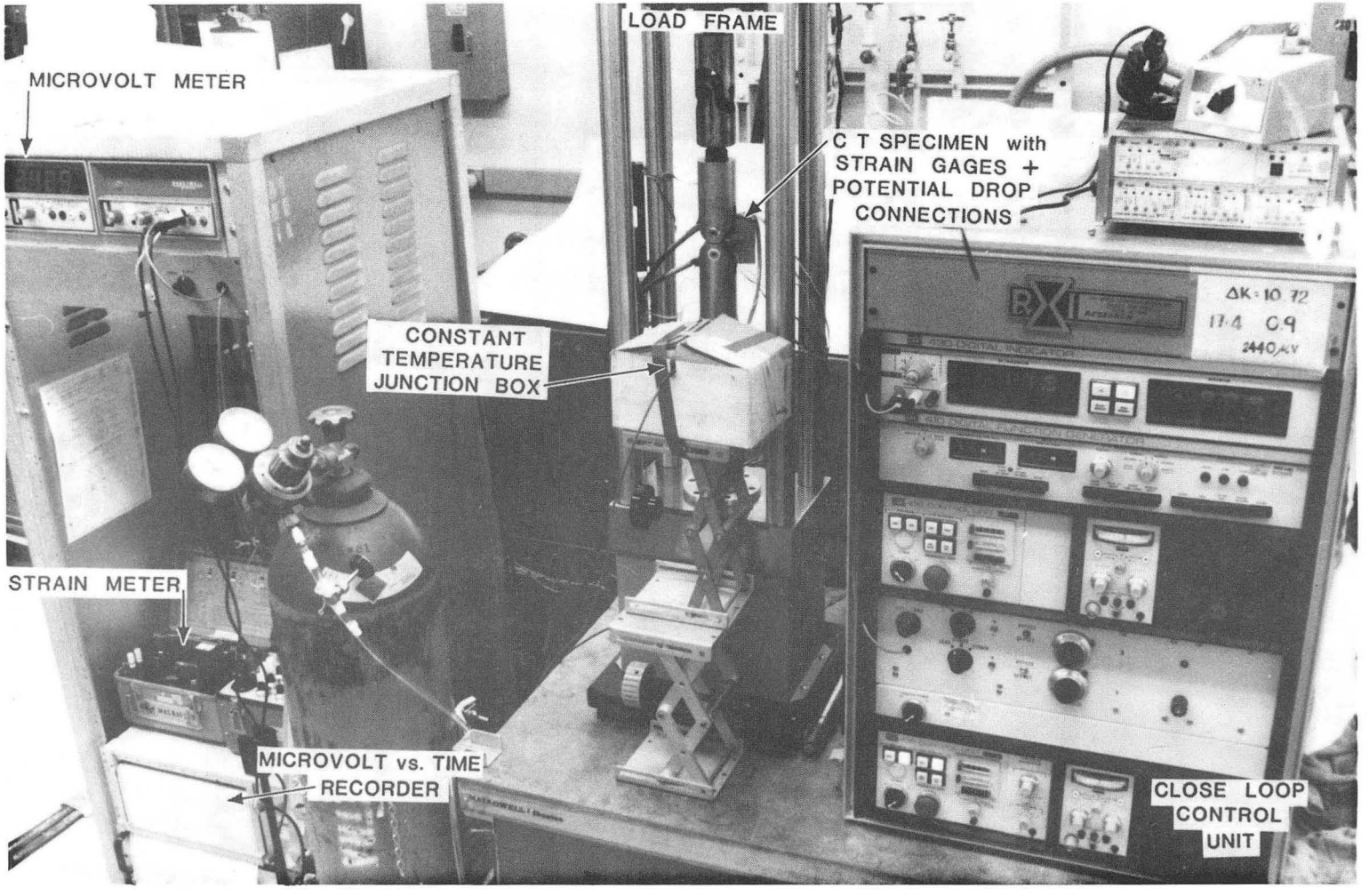

XBB 833-2255

Figure 4. Experimental set-up for fatigue crack growth test and closure measurement.

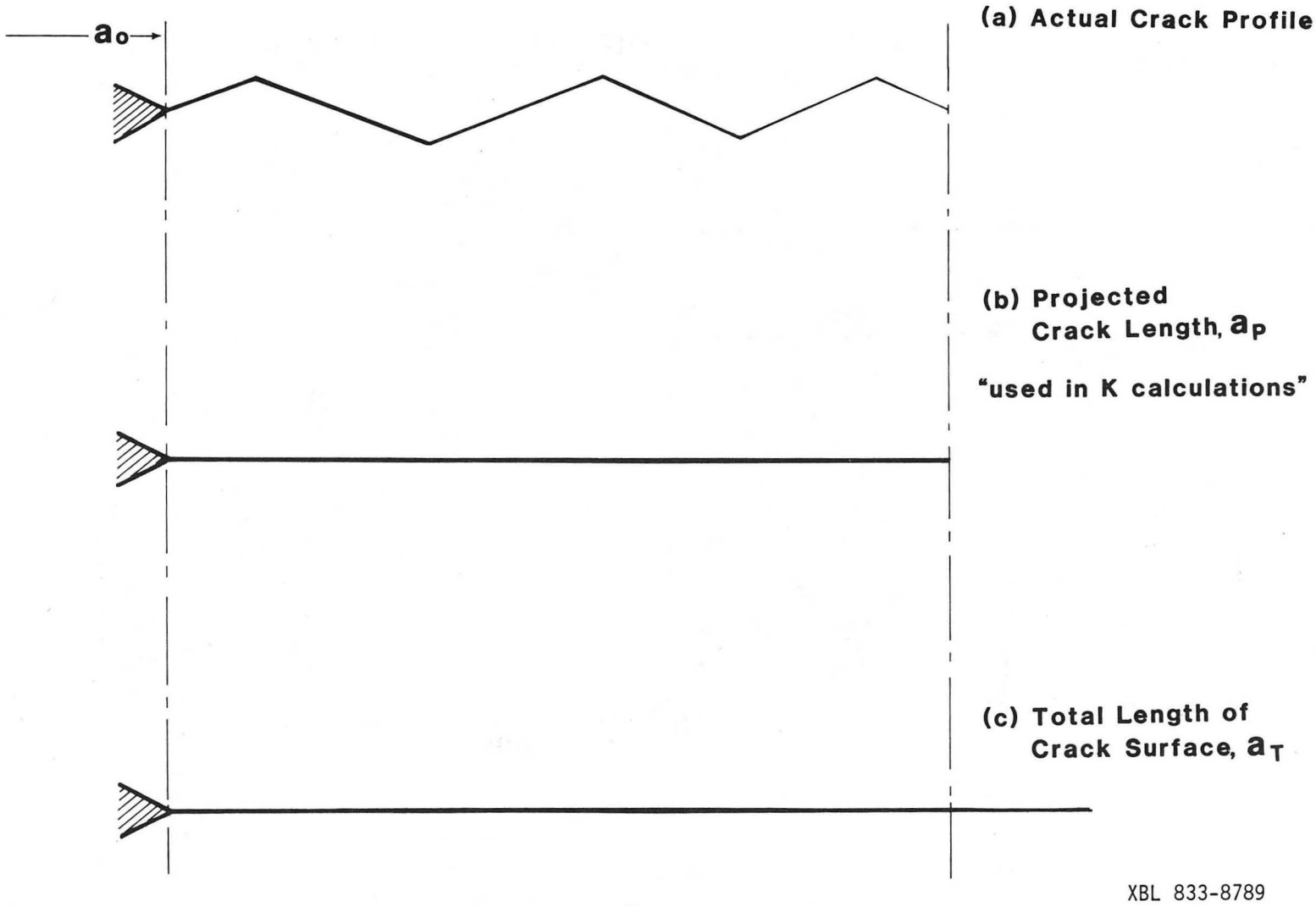

Figure 5. Schematic diagram of crack profile measurement. (a) Actual crack profile; (b) projected crack length, a_p; and (c) total length of crack surface, a_T.

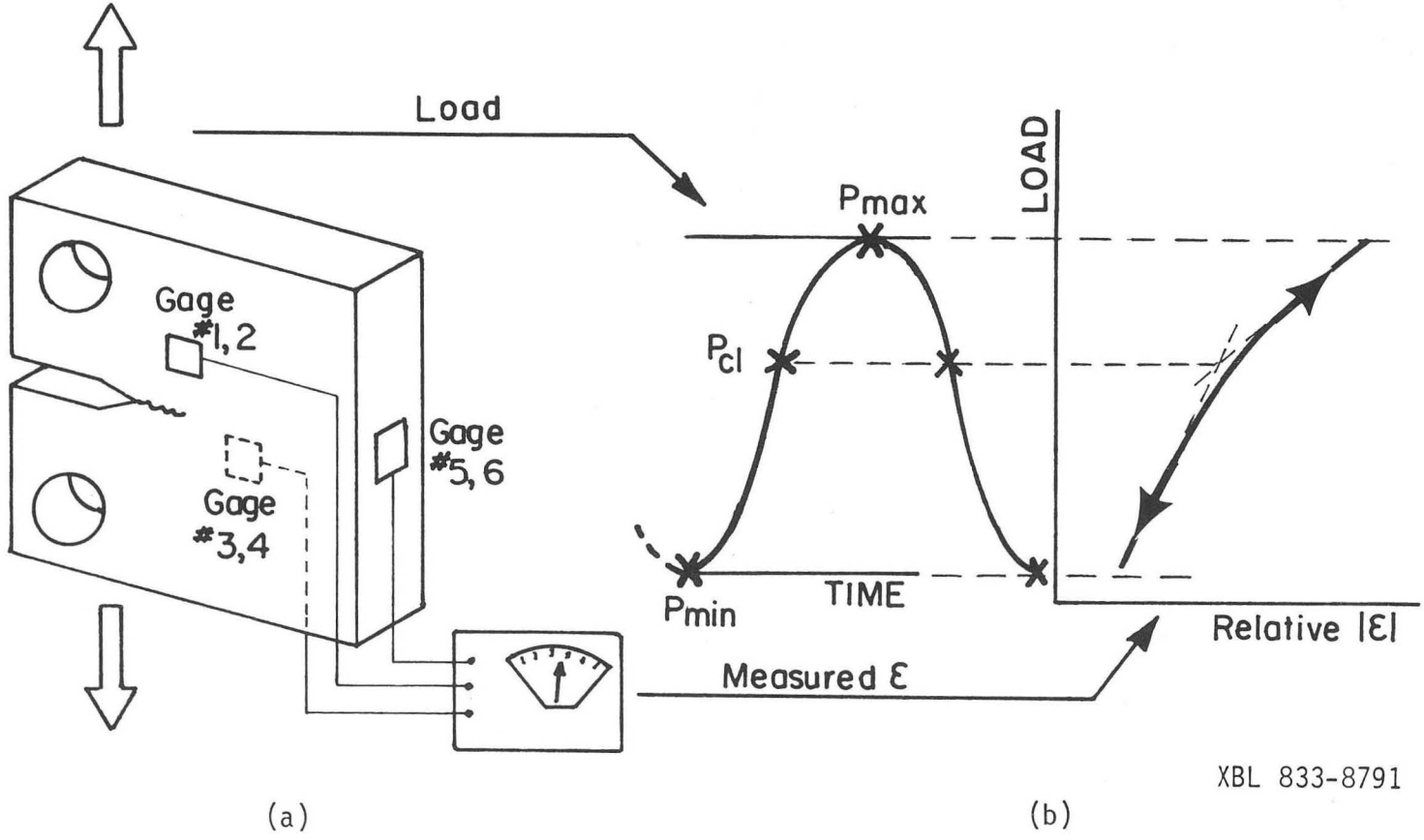

Figure 6. Closure measurements. (a) Schematic diagram of strain gage fixing and (b) relative strain, $|\varepsilon|$ vs. % load, P plot.

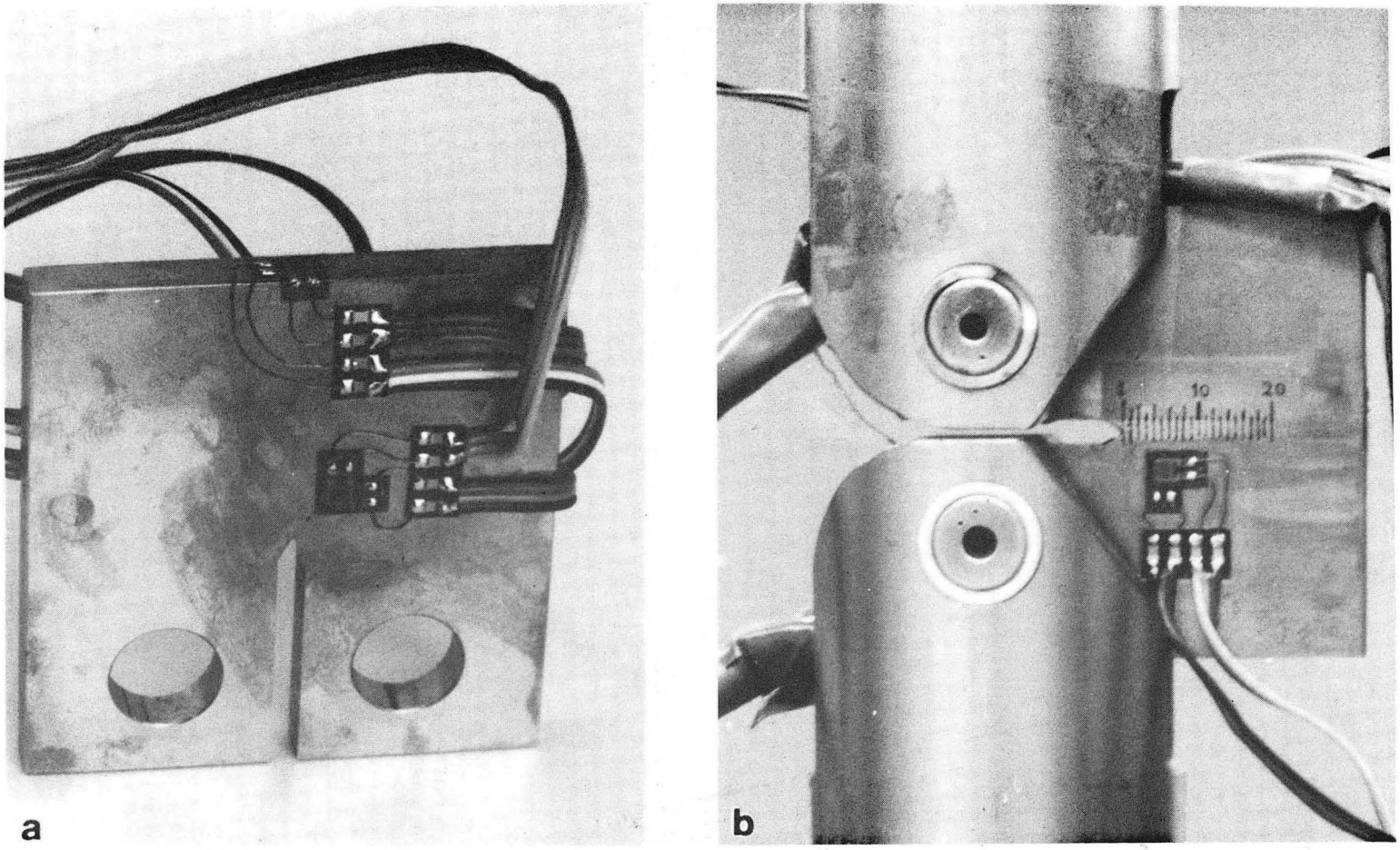

XBB 833-2254A

Figure 7. Actual arrangement of strain gages on CT specimen. (a) General view and (b) during test.

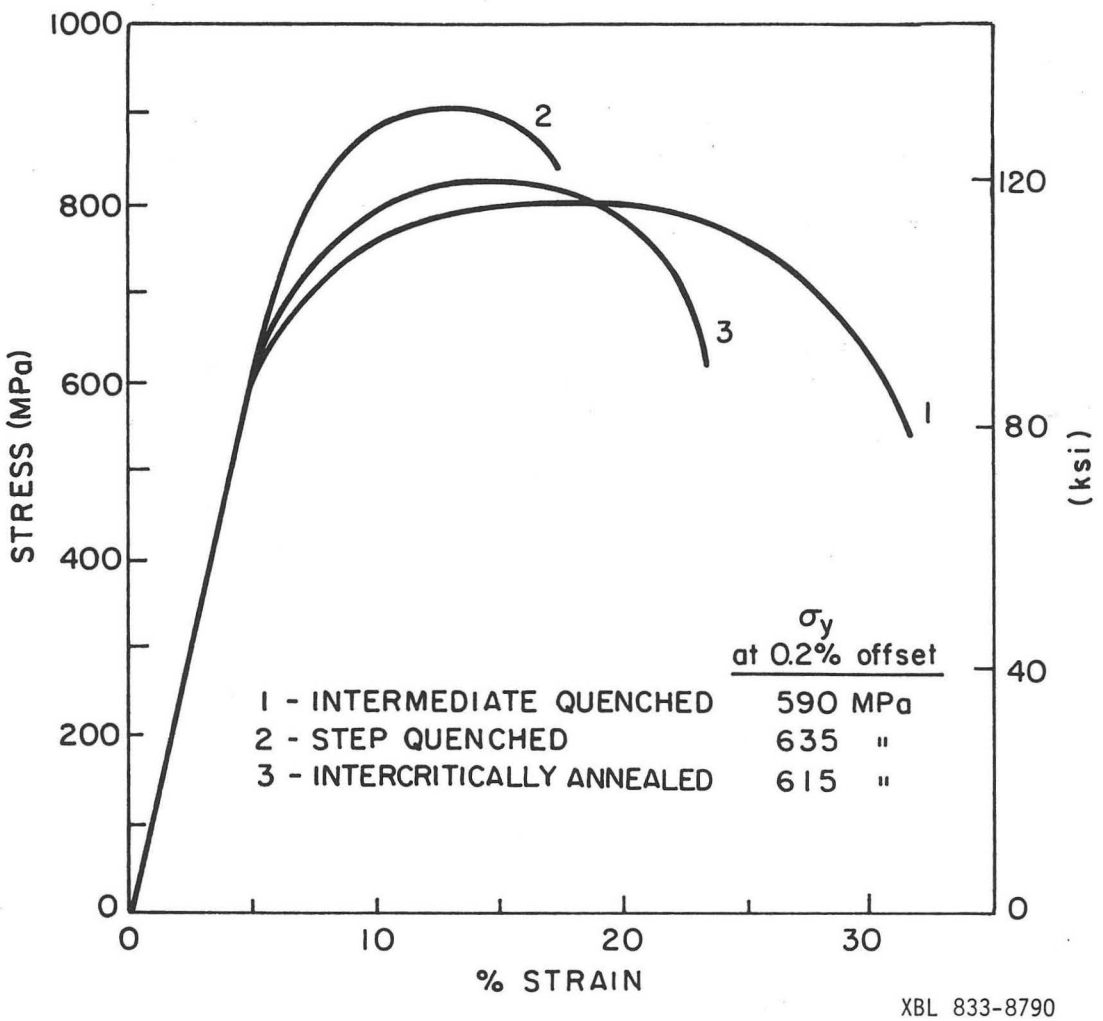

Figure 8. Engineering stress-strain curves for Fe/2Si/0.1C dual phase steel with three different microstructures.

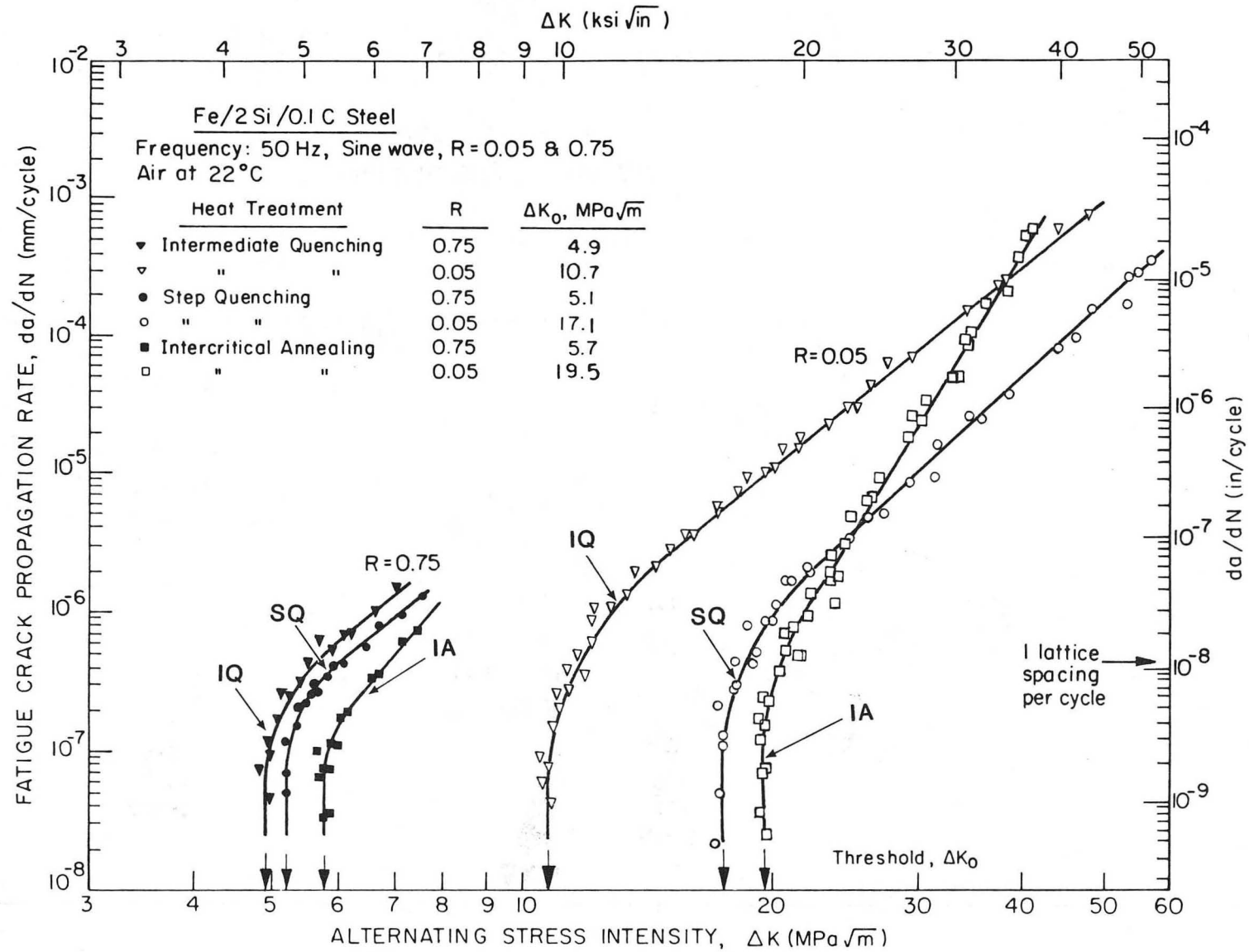

XBL 838-10897

Figure 9. Effect of microstructure on fatigue crack propagation at high (R = 0.75) and low (R = 0.05) load ratios.

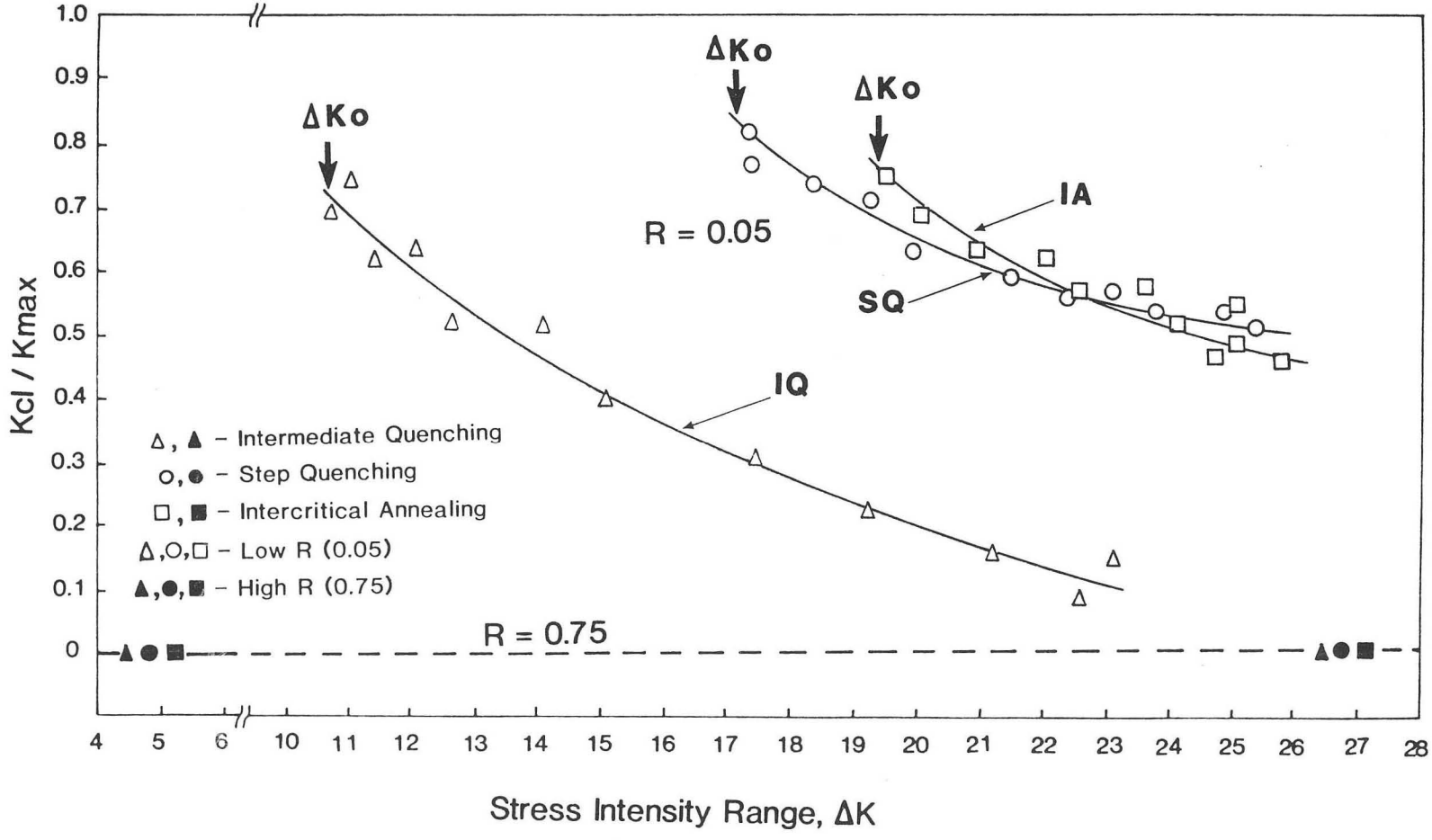

XBL 838-10896

Figure 10. Effect of microstructure and load ratio on crack closure vs. ΔK curve.

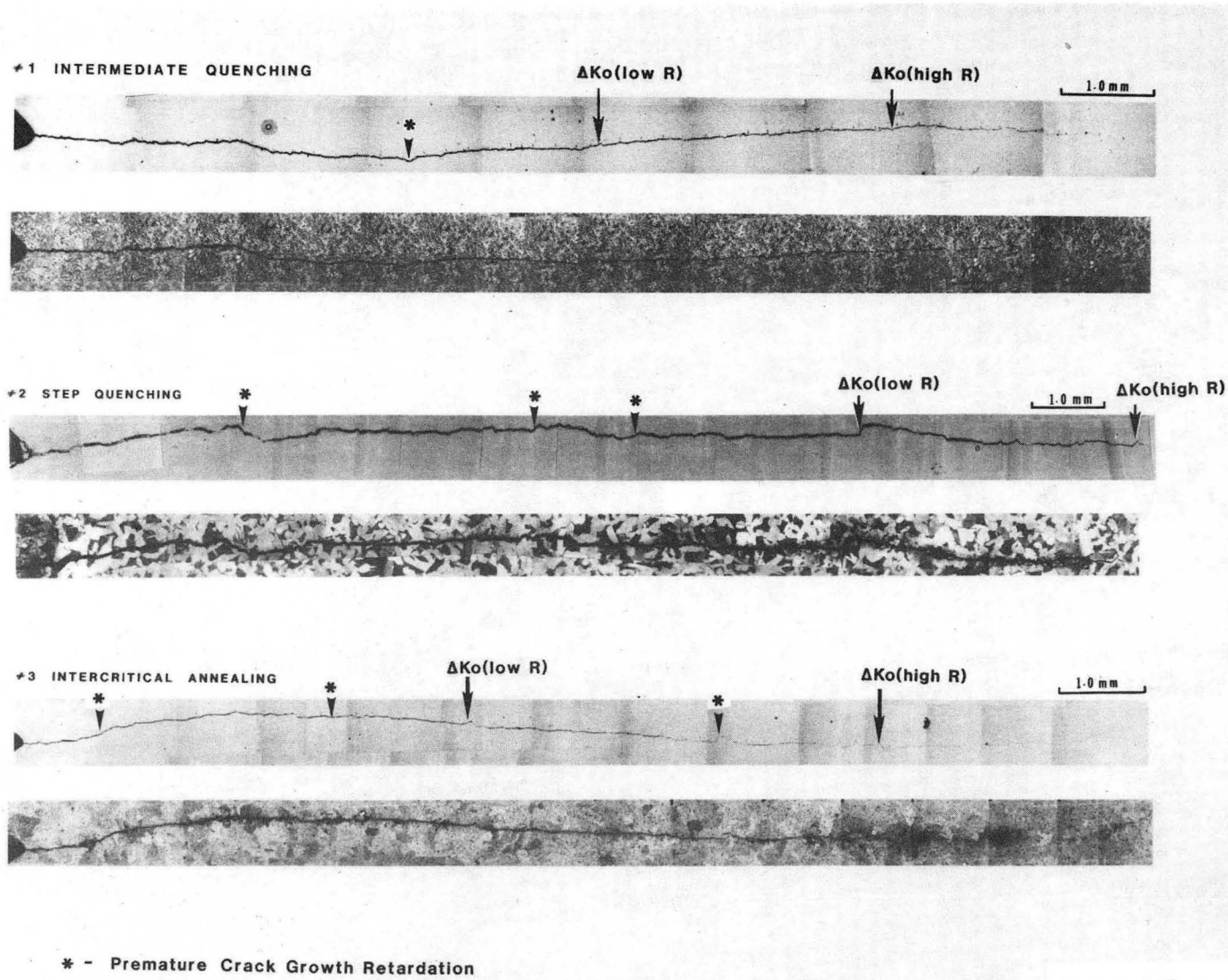

XBB 833-2301

Figure 11. Fatigue crack profiles of different microstructures at varying ΔK and load ratios for (a) IQ, (b) SQ and (c) IA.

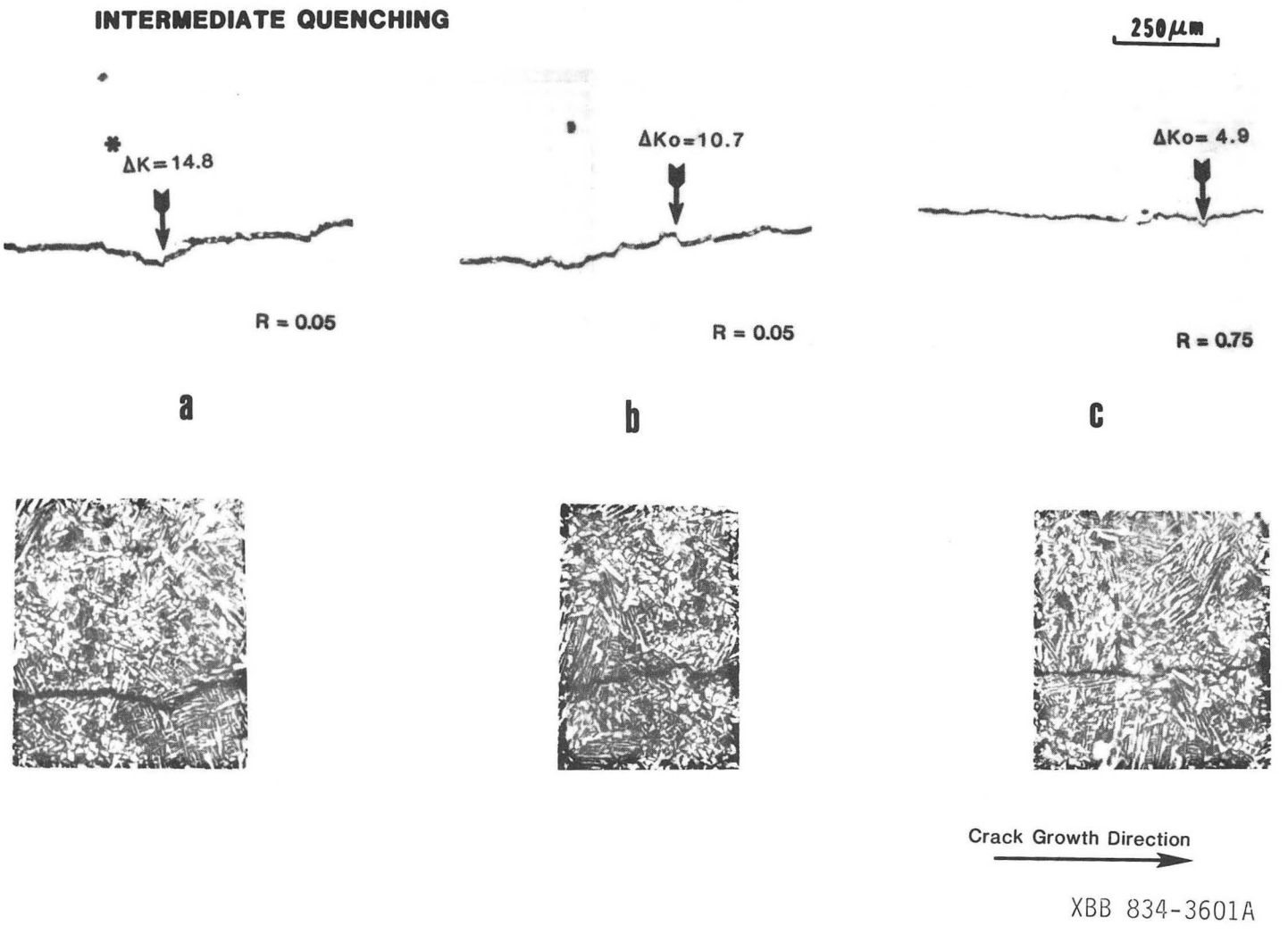

XBB 834-3601A

Figure 12. Representative crack profiles for intermediate quenching. (a)-(c) are unetched (top) and etched (bottom) micrographs at varying ΔK and R.

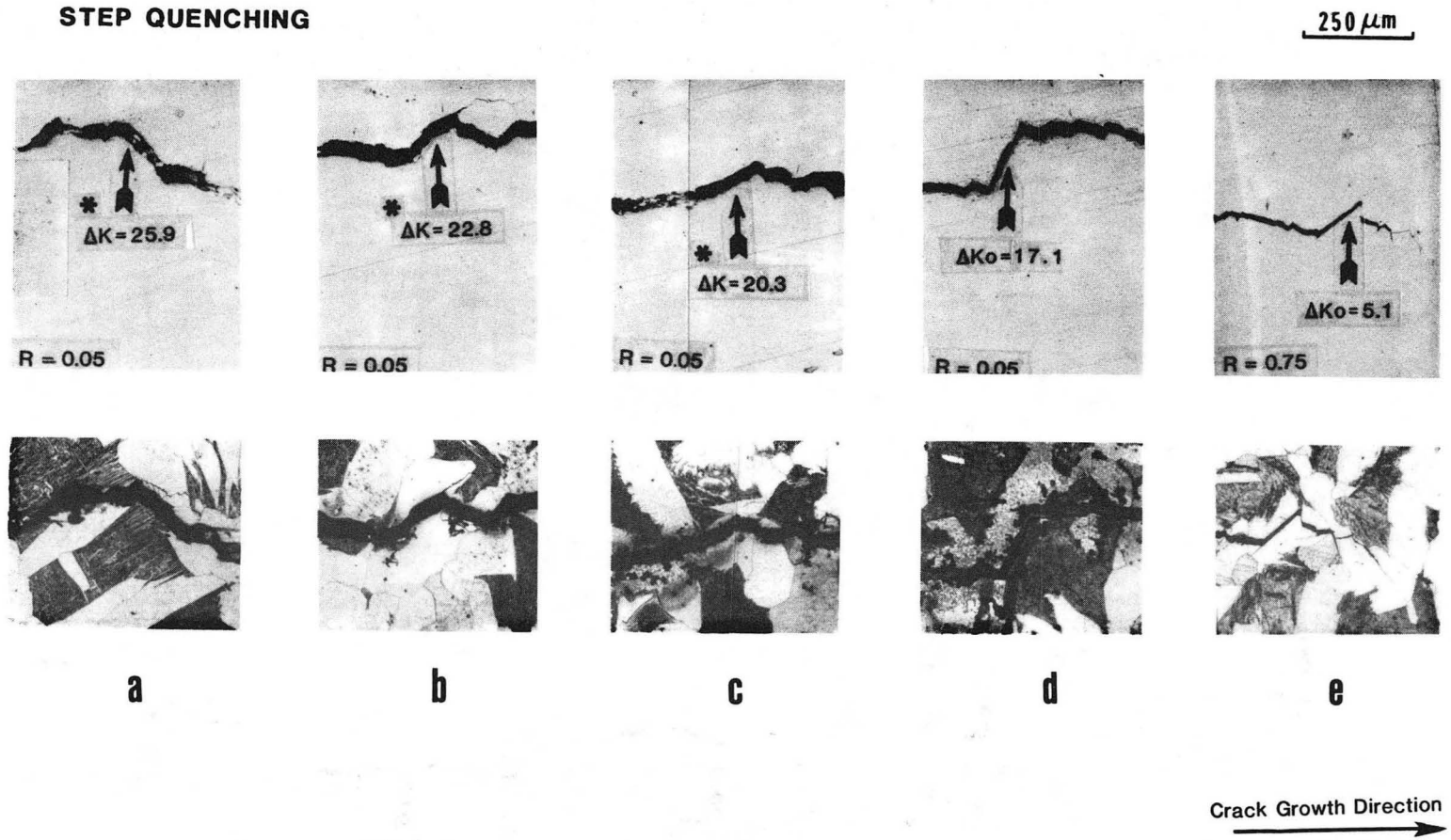

XBB 834-3602A

Figure 13. Representative crack profiles of step quenching. (a)-(e) are unetched (top) and etched (bottom) micrographs of varying ΔK and R.

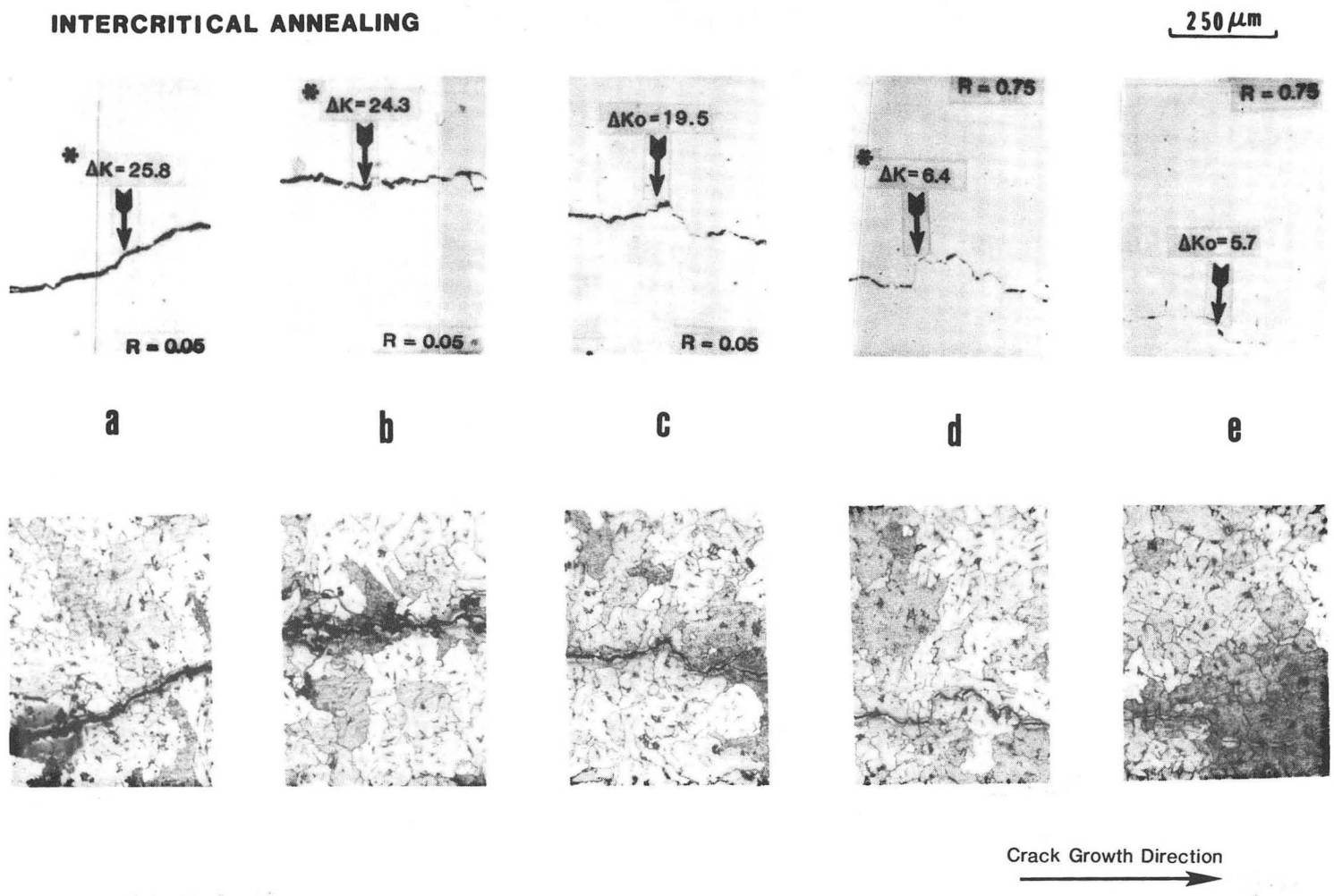

XBB 834-3206A

Figure 14. Representative crack profiles of intermediate annealing. (a)-(e) are unetched (top) and etched (bottom) micrographs of varying ΔK and R.

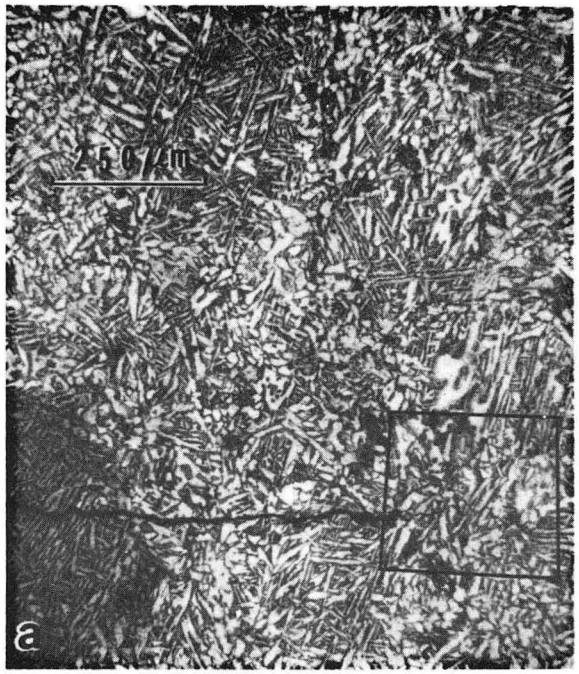

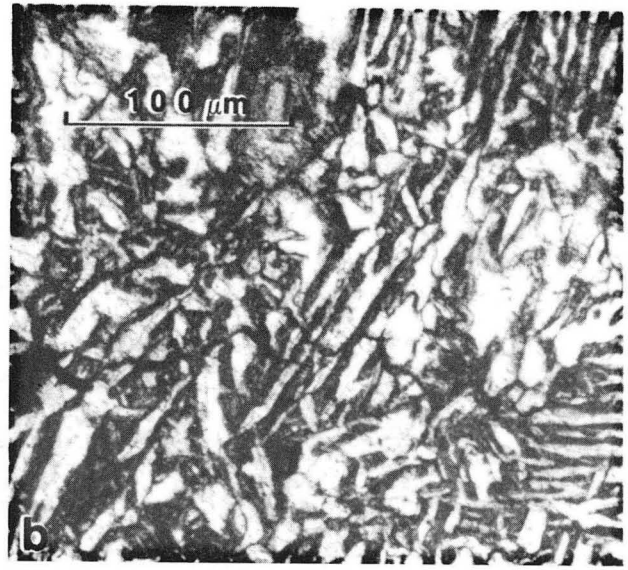

Crack Growth Direction

XBB 834-3302

Figure 15. High magnification investigation of crack path in IQ.

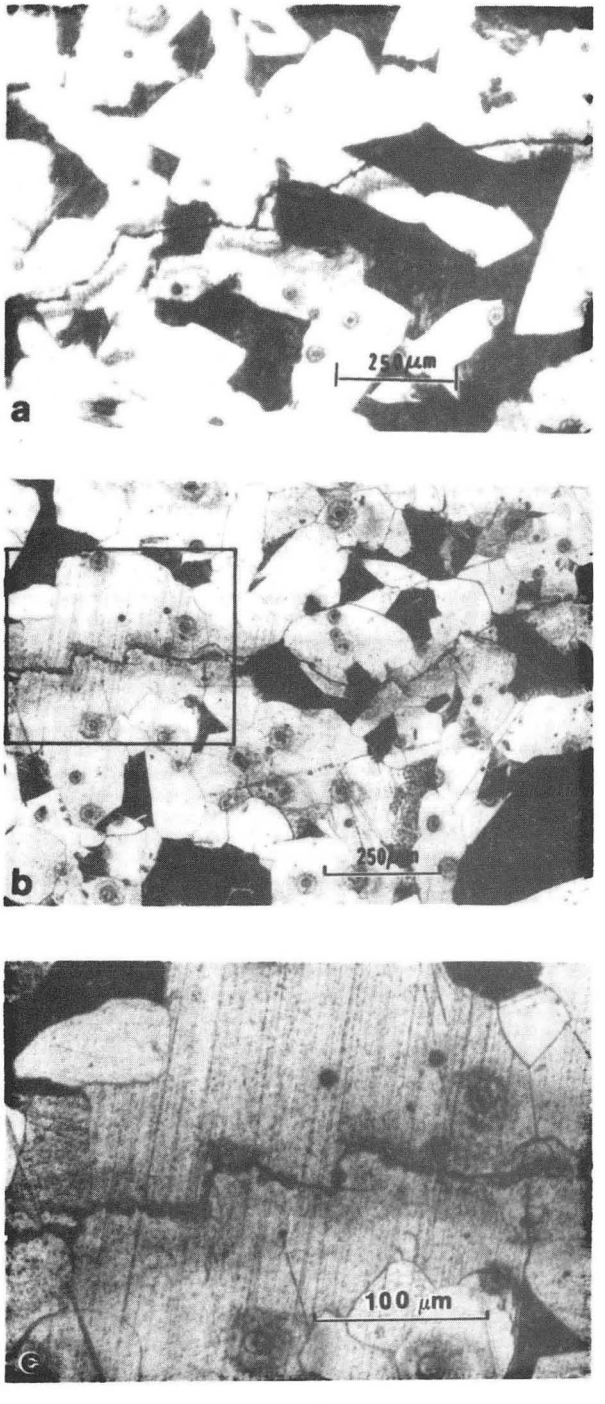

Crack Growth Direction

XBB 834-3303

Figure 16. High magnification investigation of crack path in SQ (a)-(f).

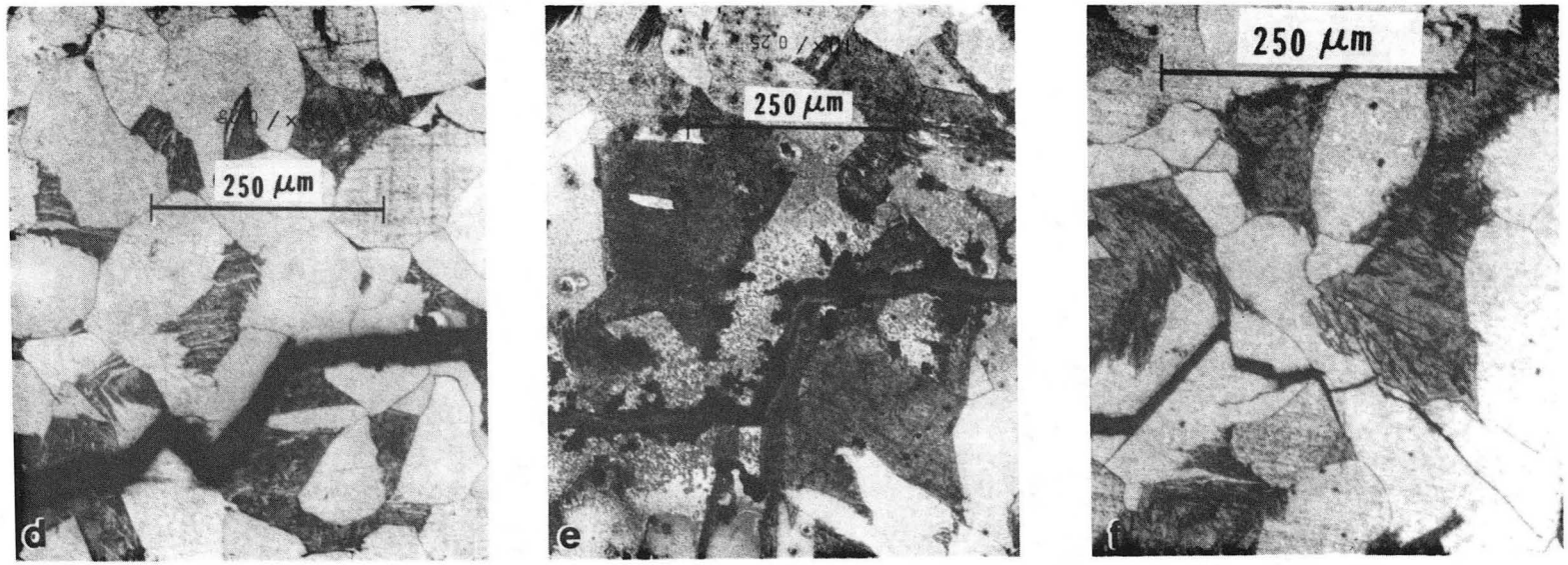

Crack Growth Direction

XBB 834-3305

Fig. 16 (Continued)

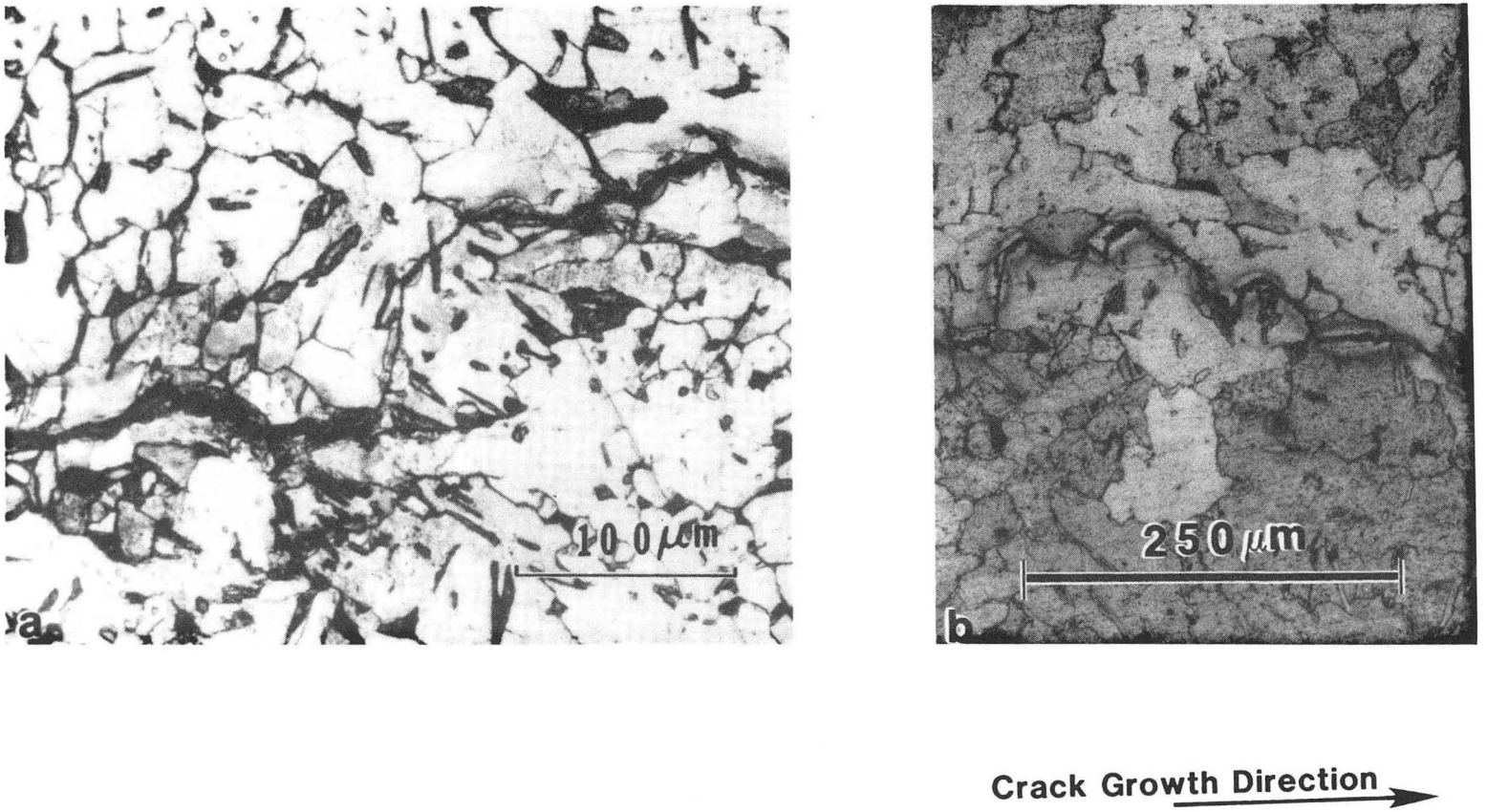

XBB 834-3304

Fig. 17. High magnification investigation of crack path in IA.

Threshold ΔKo :

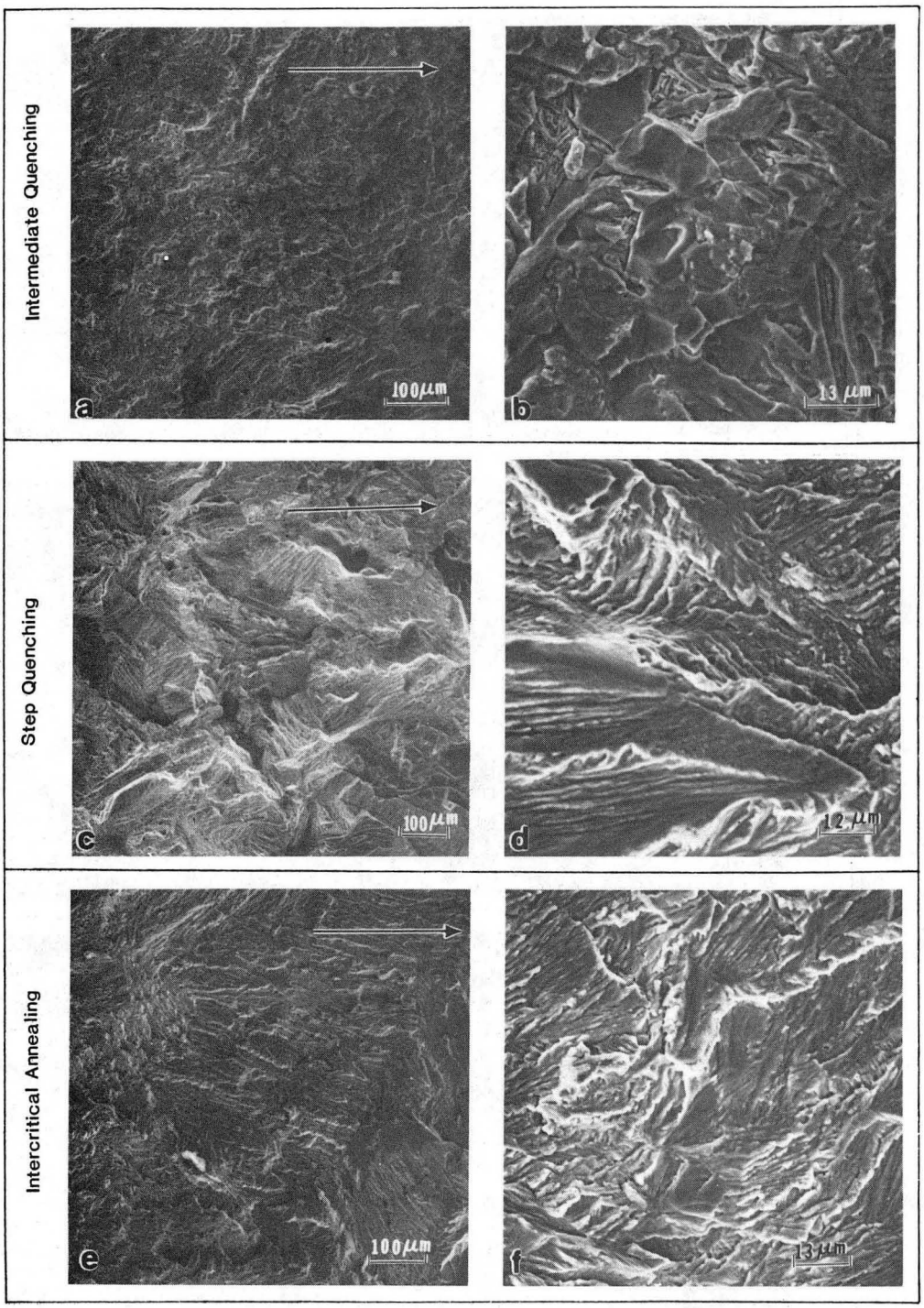

XBB 834-3600

Figure 18. SEM fractographs of IQ, SQ and IA near-threshold ΔK. (a), (c) and (e) at low magnification and (b), (d) and (f) at high magnification. The arrows indicate crack propagation direction.

Mid Growth Region :

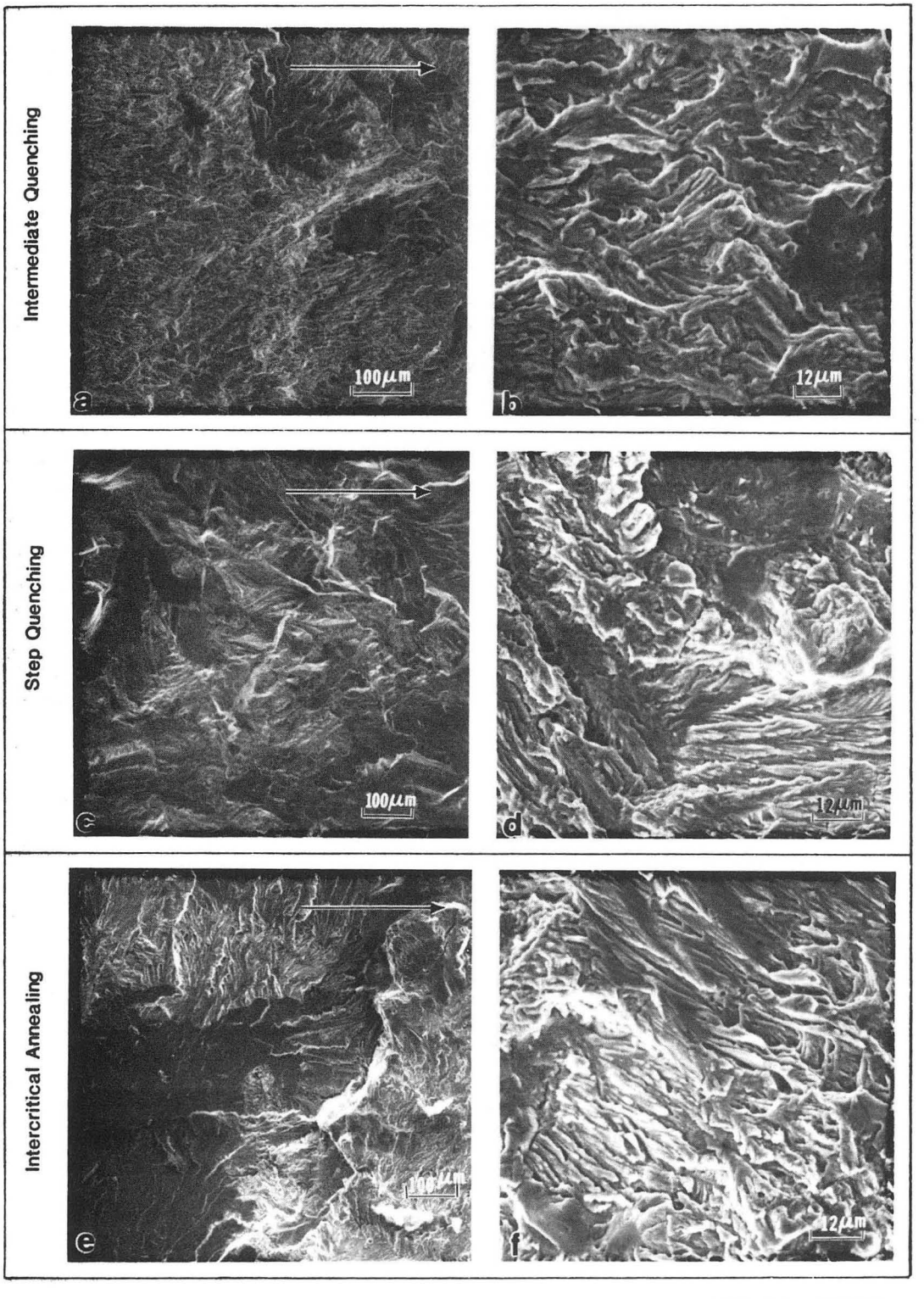

XBB 834-3599A

Figure 19. SEM fractographs of IQ, SQ and IA in mid-growth region. (a), (c) and (e) at low magnification and (b), (d) and (f) at high magnification. The arrows indicate crack propagation direction.

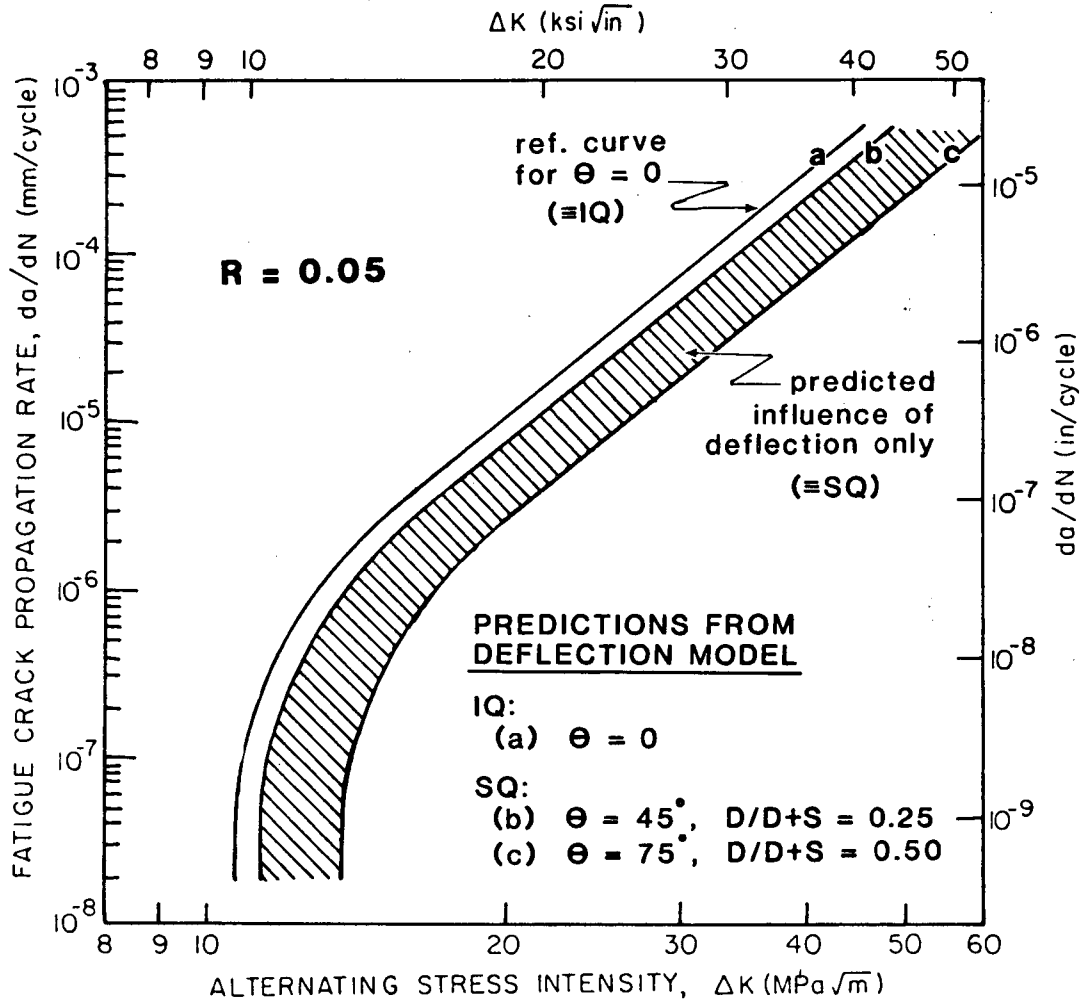

XBL 838-10894

Figure 20. Predicted growth rate behavior of the step quenched (SQ) microstructure at R = 0.05, due to crack deflection effects only.

This report was done with support from the Department of Energy. Any conclusions or opinions expressed in this report represent solely those of the author(s) and not necessarily those of The Regents of the University of California, the Lawrence Berkeley Laboratory or the Department of Energy.

Reference to a company or product name does not imply approval or recommendation of the product by the University of California or the U.S. Department of Energy to the exclusion of others that may be suitable.

TECHNICAL INFORMATION DEPARTMENT
LAWRENCE BERKELEY LABORATORY
UNIVERSITY OF CALIFORNIA
BERKELEY, CALIFORNIA 94720